The metamorphic sole of New Caledonia ophiolite: Ar-40/Ar-39, U-Pb, and geochemical evidence for subduction inception at a spreading ridge

Dominique Cluzel, Fred Jourdan, Sebastien Meffre, Pierre Maurizot, Stephane Lesimple

Crustal stacking and expulsion tectonics during continental subduction: P-T deformation constraints from Oman

Philippe Agard,[1] Michael P. Searle,[2] G. Ian Alsop,[3] and B. Dubacq[4]

[1]   The northeastern continental margin of Oman in the Saih Hatat region is characterized by high-pressure (HP) chloritoid- or carpholite-bearing metasediments and highly deformed mafic eclogites and blueschists in a series of tectonic units bounded by high-strain ductile shear zones. New data on the upper cover units of this HP nappe stack indicate that all of them underwent similar P conditions to the underlying Hulw structural unit (with a cooler exhumation pressure-temperature path). Early SSW directed crustal thickening during ophiolite emplacement created recumbent folds and strong schistose fabrics in these Permian-Mesozoic shelf carbonates and was followed by later NNE dipping normal sense shear zones and normal faults. The Mayh unit shows high strain in a 15–25 km long sheath fold that likely formed at carpholite grade pressures of 8–10 kbar. We show that there are no significant P differences across the Hulw shear zone (upper plate–lower plate discontinuity) or between the overlying Mayh, Yenkit-Yiti, and Ruwi units. Postpeak metamorphic exhumation of the HP rocks was therefore accomplished by bottom-to-SSW (rather than top-to-NNE) active footwall extrusion beneath a fixed, static, passive hanging wall. Footwall uplift beneath these passive roof faults resulted in progressive expulsion of the HP rocks from depths of ~80–90 km (eclogites) and mainly 30–35 km (blueschists and chloritoid-/carpholite-bearing units) during the Campanian–Early Maastrichtian. Oman thus provides a detailed record of how continental material (thick platform shelf carbonates) progressively jammed a subduction zone and emphasizes the contrasting behavior between cover units and their underlying basement. **Citation:** Agard, P., M. P. Searle, G. I. Alsop, and B. Dubacq (2010), Crustal stacking and expulsion tectonics during continental subduction: P-T deformation constraints from Oman, *Tectonics*, *29*, TC5018, doi:10.1029/2010TC002669.

1. Introduction

[2]   High-pressure (HP) and ultrahigh pressure (UHP) continental rocks occur along plate boundaries and have been reported, since the discovery of coesite [*Chopin*, 1984], in most collisional mountain belts formed during the Phanerozoic. These range from Paleozoic mountain belts such as the Kokchetav massif, Kazakhstan [e.g., *Zhang et al.*, 1997] and the Western Gneiss Region, Norway [*Wain*, 1997] through the Triassic Dabie Shan–Sulu belt, China [e.g., *Hacker et al.*, 1995] to the Late Cretaceous–Tertiary Alpine–Himalayan belt [*Chopin et al.*, 1991; *O'Brien et al.*, 2001].

[3]   Continental subduction is a highly transient process (1–10 Ma) at the end of which the buoyant continental crust is exhumed with velocities comparable to those of plate tectonics at mantle depths (1–5 cm/yr) and later decelerates (~mm/yr) in the upper crust (Western Alps [*Duchêne et al.*, 1997; *Rubatto and Hermann*, 2001], Papua [*Baldwin et al.*, 2004], Himalayas [*O'Brien*, 2006; *Parrish et al.*, 2006], Dabie Shan [*Liu et al.*, 2006], Kokchetav [*Hermann et al.*, 2001; *Hacker et al.*, 2003]). Since the pioneering study of *Chemenda et al.* [1995, 1996], the exhumation of continental rocks is thus generally regarded as buoyancy driven. Recent studies suggested that large UHP terranes may indeed be exhumed as thick crustal slabs (e.g., Western Gneiss Region, Norway [*Kylander-Clark et al.*, 2008; *Hacker et al.*, 2010]). Yet, as noted by *Jolivet et al.* [2005], many exhumed HP-UHP thrust sheets are notably thinner (~100 m to a few kilometers) than the thickness of normal crust. In the Western Alps for example, the UHP Dora Maira unit (~3.5 GPa, 750°C [*Chopin et al.*, 1991]) is juxtaposed and sandwiched with basement and cover slices that underwent significantly lower P conditions (~1.5 GPa −550°C [*Michard et al.*, 1993]). The picture can thus be more complex than that of a simple extrusion of continental crust, and the way in which these units return to the surface needs to be tracked in more detail to gain insights into mechanical processes at work during continental subduction [e.g., *Ernst*, 2001].

[4]   Since continental subduction was not followed by collision, nowhere are the exposures of HP rocks so completely well preserved as along the northeastern continental margin of Oman in the Saih Hatat region (Figures 1a and 1b) [*Goffé et al.*, 1988; *El-Shazly et al.*, 1990; *Searle et al.*, 1994, 2004; *Gregory et al.*, 1998; *Miller et al.*, 1999, 2002; *Gray et al.*, 2004a, 2004b; *Yamato et al.*, 2007; *Warren and Miller*, 2007]. Coupled with the unique, almost complete exposures and preservation of the HP units along northern Saih Hatat in Oman, precise U-Pb age data both for the ophiolite and eclogite rocks are available [*Warren et al.*, 2003, 2005], together with Ar-Ar and Rb-Sr ages

[1]ISTEP, UMR 7193, UPMC Paris 06, CNRS, Paris, France.
[2]Department of Earth Sciences, Oxford University, Oxford, UK.
[3]Department of Geology and Petroleum Geology, School of Geosciences, University of Aberdeen, Aberdeen, UK.
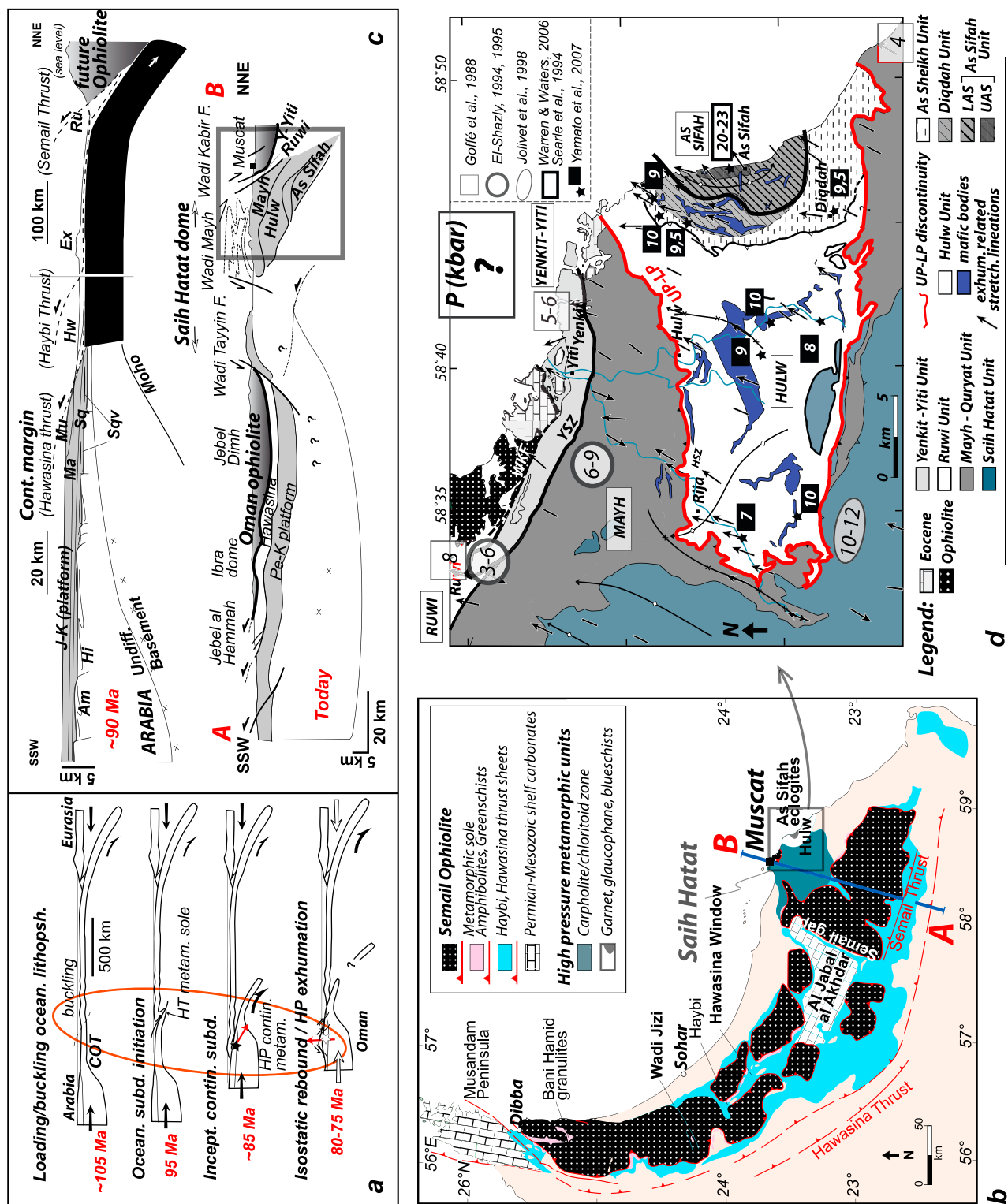[4]Department of Earth Sciences, Cambridge University, Cambridge, UK.

Figure 1

[*El-Shazly and Lanphere*, 1992; *Searle et al.*, 1994; *Hacker et al.*, 1996; *Miller et al.*, 1999; *El-Shazly et al.*, 2001] and recently published detailed exhumation paths [*Yamato et al.*, 2007].

[5] Most studies, however, have so far been focused on the lower (eclogite) part of the HP nappe stack [e.g., *El-Shazly et al.*, 1990, 1997; *Warren and Waters*, 2006; *Yamato et al.*, 2007]. The aim of this paper is thus to provide pressure-temperature (P-T) estimates for the upper units of the HP nappe stack in the light of exhumation-related fabrics seen in the field [e.g., *Michard et al.*, 1994; *Jolivet et al.*, 1998]. We then combine the P-T estimates of the whole stack of nappes to further constrain both burial and exhumation tectonics during continental subduction.

2. Geological Setting of the HP Nappe Stack

2.1. HP Metamorphism: Obduction-Related Continental Subduction

[6] The Saih Hatat HP nappes crop out below a portion of the oceanic lithosphere obducted onto Arabia almost synchronously along thousands of kilometers [*Coleman*, 1971, 1981; *Ricou*, 1971] (Figure 1a). This large-scale obduction remains a puzzling geodynamic process and conflicting interpretations have been published [*Boudier et al.*, 1988; *Nicolas*, 1989; *Hacker et al.*, 1996; *Searle and Cox*, 1999; *Breton et al.*, 2004]. Increasing evidence shows that these ophiolites correspond to suprasubduction zone ophiolites [e.g., *Pearce et al.*, 1981; *Shervais*, 2001] originating from a newly formed subduction zone in the southern Neo-Tethyan domain [*Searle et al.*, 2004, 2005; *Agard et al.*, 2007].

[7] HP-LT metamorphism in Oman is classically considered to have accompanied the later stages of the obduction process (Figure 1a), which initiated at ~95 Ma and were over by ~70 Ma [*Lippard*, 1983; *Michard et al.*, 1983; *Goffé et al.*, 1988; *Searle and Cox*, 1999; *El-Shazly et al.*, 2001; *Warren et al.*, 2003, 2005]. However, whereas *Goffé et al.* [1988] and *Searle et al.* [2004] relate the HP-LT metamorphic imprint to the NE directed subduction of the leading edge of the Arabian continental margin below the ophiolite, and exhumation patterns to reverse movements taking place along the subduction plane, *El-Shazly et al.* [2001] and *Breton et al.* [2004] relate the HP-LT imprint
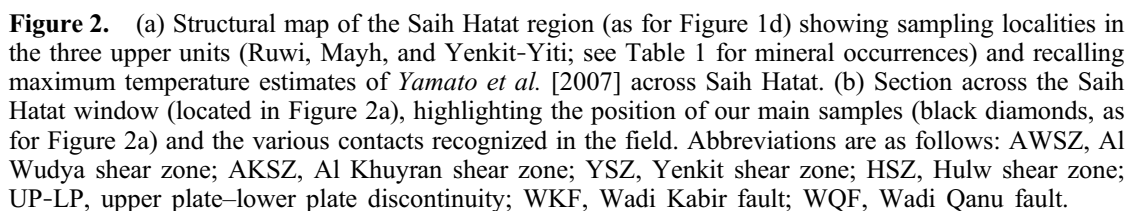
to the existence of an additional, NE dipping intracontinental subduction isolating a North Muscat microplate. *Gregory et al.* [1998], *Gray et al.* [2000, 2004a, 2004b], and *Gray and Gregory* [2003], on the other hand, suggested that the HP event involved an earlier intracontinental subduction (~130–90 Ma) dipping to the SW under the Arabian passive margin, based on the distribution of a few older (preophiolite) Ar-Ar ages.

[8] Biostratigraphic and recent radiometric age constraints (Rb-Sr [*El-Shazly et al.*, 2001]; U-Pb [*Warren et al.*, 2003, 2005]) lend support to the scenario of a single subduction zone active during ~25 Myr, ending through continental subduction of the Arabian margin between 85 and 80 and 70 Ma. Despite ongoing controversy [*Gray et al.*, 2005; *Searle et al.*, 2005; *Warren and Miller*, 2007], we note that the restoration of *Searle et al.* [2004] was recently supported by high resolution P-T data for the central Hulw unit [*Yamato et al.*, 2007].

2.2. Tectonic Setting at the Start of Continental Subduction

[9] In this paper we assume the existence of a single NE dipping subduction zone and show that the whole geodynamic and exhumation history, as seen from deformation patterns and P-T data, can be derived from a relatively simple paleogeography. The lithostratigraphy of the rocks from the HP nappe stack is well constrained and detailed in numerous publications [e.g., [*Glennie et al.*, 1974; *Béchennec et al.*, 1990; *Robertson and Searle*, 1990; *Miller et al.*, 2002; *Breton et al.*, 2004; *Scott*, 1990; *Searle et al.*, 2004; *Searle*, 2007; *Chauvet et al.*, 2009]. Below the major regional unconformity of Late Maastrichtian age (68–65 Ma), which overlies all allochthonous units throughout north Oman, one finds, from bottom to top (1) "basement" rocks represented by Upper Proterozoic to Paleozoic metasedimentary series; these latter series include a succession of upper Proterozoic to lower Cambrian greenschist facies greywackes, shales and cherts (at least 2500 m thick; termed the Hatat schists), overlain by 500 m of gray and yellow dolostone (Hijam Formation), in turn overlain disconformably by a massive unit of Ordovician quartzites (Amdeh Formation, up to 2300 m thick); (2) Permian-Triassic rocks intruded by mafic sills associated with the Neotethyan rifting; and (3) Permian-

Figure 1. (a) Sketch illustrating the Late Cretaceous geodynamic evolution of northern Oman, whereby continental subduction of the Arabian margin develops through obduction of the Oman ophiolite (adapted from *Agard et al.* [2007]). (b) Simplified structural map of northern Oman, (modified from *Searle* [2007]). High-pressure low-temperature rocks are only found south of Muscat, in the Saih Hatat region, to the east of the Semail gap. (c) Comparison of the restored section across the continental passive margin of Oman during the Late Cretaceous (data from *Michard et al.* [1994], *Miller et al.* [1998, 2002], *Searle et al.* [2004], and *Chauvet et al.* [2009]) and of the present-day cross section. The AB transect is located in Figure 1b. Formation abbreviations are as follows: Am, Amdeh; Ex, Oman Exotics; Hi, Hijam; Hw, Hawasina; Ma, Mahil; Mu, Muti; Ru, Ruwi; Sq, Saiq; Sqv, Saiq volcanics. See text for age constraints. The Muti, Haybi, and Ruwi formations are important Late Cretaceous time equivalent units. A close-up view of the northern part of this section is shown in Figure 2b (frame with the five main structural metamorphic units indicated). (d) Structural map of the Saih Hatat region showing the main structural metamorphic units (boxes: Ruwi, Mayh, Yenkit-Yiti, Hulw, and As Sifah units) and the location of some of the major ductile shear zones discussed in the text (HSZ, Hulw shear zone; YSZ, Yenkit shear zone). The so-called upper plate–lower plate discontinuity (UP-LP), which is equivalent to the HSZ, is outlined in red. Contrasting pressure estimates (P, in kbar) obtained by earlier workers are indicated. Arrows correspond to exhumation-related stretching lineations [after *Yamato et al.*, 2007, and references therein]. Major fold axes are also shown.

Figure 2. (a) Structural map of the Saih Hatat region (as for Figure 1d) showing sampling localities in the three upper units (Ruwi, Mayh, and Yenkit-Yiti; see Table 1 for mineral occurrences) and recalling maximum temperature estimates of *Yamato et al.* [2007] across Saih Hatat. (b) Section across the Saih Hatat window (located in Figure 2a), highlighting the position of our main samples (black diamonds, as for Figure 2a) and the various contacts recognized in the field. Abbreviations are as follows: AWSZ, Al Wudya shear zone; AKSZ, Al Khuyran shear zone; YSZ, Yenkit shear zone; HSZ, Hulw shear zone; UP-LP, upper plate–lower plate discontinuity; WKF, Wadi Kabir fault; WQF, Wadi Qanu fault.

Triassic to Upper Cretaceous shelf carbonates. No basement rock proper crops out in the Saih Hatat window, however. Figure 1c shows a restored cross section assuming a simple paleogeographic setting with NE dipping intraoceanic subduction ultimately leading to continental subduction [*Robertson and Searle*, 1990; *Searle et al.*, 2004; *Agard et al.*, 2007; *Warren and Miller*, 2007].

[10] Initial Neo-Tethyan rifting, block faulting and subsidence had resulted, by the late Permian, into a vast stable shelf carbonate platform (Saiq Formation) which lasted throughout the Triassic (Mahil Formation), Jurassic (Sahtan Group), Early Cretaceous (Kahmah Group) and Aptian-Cenomanian (Wasia Group). Outboard of the shelf carbonates (Figure 1c), slope facies (Sumeini Group) and proximal basin facies rocks (Hamrat Duru Group; Hawasina complex) in the lower allochthon are lateral, age-equivalent units. Two volcanic horizons (Sq1v and Sq2v) comprising mildly alkaline volcanic flows and rhyolitic tuffs, lies within the Middle–Late

Table 1. List of Mineral Occurrences in the Main Samples Studied Here (located in Figure 3)[a]

Sample[b]	Unit	Mineral Occurrences									
		Q	Chl	Phg	Prl	Kln	Prg	Car	Ctd	Op	Rt
R 7.07	Ruwi	x	x	x				r	x	x	x
R 7.23	Ruwi	x		x		x	x			x	x
R 7.24	Ruwi	x	x	x				x		x	x
Y 7.08	Yenkit-Yiti	x		x	x	x				x	x
Y 7.09	Yenkit-Yiti	x		x	x					x	x
Y 7.18	Yenkit-Yiti	x		x	x	x				x	x
M 7.20	Mayh	x	x	x				r	x	x	x
M 7.25	Mayh	x	x	x						x	
M 5.29	Mayh	x	x	x			x	r	x	x	x
M 5.11	Mayh	x	x	x				r		x	x
M 5.35	Mayh	x	x	x				r		x	x
SF 7.03	Mayh (SFA)	x		x	x					x	
SF 7.04	Mayh (SFA)	x	x	x	x			r?		x	

[a]Abbreviations are as follows: Car, carpholite; Chl, chlorite; Ctd, chloritoid; Kln, kaolinite; Op, opaque minerals; Phg, phengites; Prg, paragonite; Prl, pyrophyllite; Q, quartz; Rt, rutile. Key to symbols: x refers to a fresh mineral; r refers to a mineral that is (at least partially) replaced.
[b]Bold font indicates samples for which P-T estimates are provided.

Permian Saiq Formation [*Le Métour et al.*, 1986a, 1986b]. Stable sedimentation along the north Arabian platform ended abruptly at the end of the Cenomanian, 90 Ma ago, when the passive margin was flexed down to form the Aruma foreland basin filled with Muti and Fiqa formations [*Glennie et al.*, 1973, 1974; *Warburton et al.*, 1990]. Between 88 and 70 Ma (Coniacian-Campanian) the thrust sheets of the Hawasina and Haybi complexes, of the Ruwi melange and of the Semail ophiolite were emplaced into the basin and on top of the shelf carbonates.

2.3. Upper Plate–Lower Plate Discontinuity

[11] Considerable structural analysis of the Saih Hatat already exist in the literature, and the reader is referred to previous mappings and detailed observations by *Le Métour et al.* [1986a, 1986b], *Searle et al.* [1994, 2004], *Miller et al.* [2002], and *Chauvet* [2007] and to additional investigations [*Michard et al.*, 1994; *Jolivet et al.*, 1998; *Warren and Miller*, 2007; *Yamato et al.*, 2007].

[12] A sharp discontinuity in deformation style, quartz deformation microstructures and stratigraphy [*Miller et al.*, 2002; *Chauvet*, 2007; *Chauvet et al.*, 2009] occurs along the so-called "upper plate–lower plate discontinuity" [*Miller et al.*, 2002] (which coincides with the Hulw shear zone; Figures 2a and 2b). Whatever the interpretation of this contact [*Gray et al.*, 2005; *Searle et al.*, 2005], and irrespective of minor mapping differences (see detailed comparisons in the work by *Warren and Miller* [2007] and *Yamato et al.* [2007]), all authors agree on the existence of a contrast, possibly in tectonometamorphic evolution, between the lower (e.g., As Sifah, Hulw) and the upper units of the HP nappe stack (from top to bottom: the Yenkit-Yiti, Ruwi, and Mayh units; Figure 2b). All these units are dominantly cover derived, spanning the Amdeh to Permian for the lower ones and the Permian to Upper Cretaceous for the upper ones. Note, however, that the Yenkit-Yiti and

Mayh units are platform series, whereas the Ruwi unit is an Upper Cretaceous melange (Figure 1c) [*Le Métour et al.*, 1986a, 1986b; *El-Shazly and Coleman*, 1990]).

[13] The deformation style is markedly different in the upper units, with less stretching and boudinage and an overall less intense finite deformation [*Gray et al.*, 2005], except in the sheath fold hinges of southern Wadi Mayh [*Miller et al.*, 2002; *Searle et al.*, 2004]. Two main shear zones, the Yenkit shear zone and the Wadi Qanu fault, separate the Yenkit-Yiti, Ruwi, and Mayh units (Figure 2b). Within the Mayh unit, *Searle et al.* [1994] reported the existence of ductile to brittle shear zones with top to the SW transport direction (the Al Wudya and Al Khuryan shear zones; Figure 2b). Exhumation patterns and shear senses are also clearly top to the NE for *Jolivet et al.* [1998] or *Chauvet et al.* [2009] and dominantly top to the NE, yet more coaxial for *Michard et al.* [1994] and *Miller et al.* [2002]. Early south directed shear senses were reported by *Michard et al.* [1994] but contested by *Miller et al.* [2002].

[14] Only few P-T data exist on the uppermost, external Ruwi, Yenkit-Yiti, and Mayh units (Figure 2a). For the Ruwi unit, peak P-T estimates vary between 8 kbar at 180°C–250°C [*Goffé et al.*, 1988] and 3–6 kbar at 250°C–315°C [*El-Shazly and Coleman*, 1990; *El-Shazly*, 1994, 1995], with conflicting P-T claims [*Vidal and Theye*, 1996; *El-Shazly*, 1995]. For the Mayh unit, they vary between 4 and 6 kbar [*Goffé et al.*, 1988], 6–9 kbar [*El-Shazly*, 1995] and 11–12 kbar [*Jolivet et al.*, 1998]. *El-Shazly* [1994, 1995] therefore concluded that a down-section increase in pressure and metamorphic grade across these upper plate units (his regions I and II) existed. P-T paths were either considered clockwise [*El-Shazly*, 1995] or anticlockwise [*Goffé et al.*, 1988].

[15] P-T constraints are therefore sorely lacking in order to (1) determine possible pressure gaps across the various shear zones and the nature of the contrast on either side of the upper-lower plate and (2) constrain burial/exhumation scenarios and better understand continental subduction processes.

3. Petrology and Structural Patterns in the Upper Units

[16] Sampling focused on the metapelitic layers of the uppermost units, mainly on a N–S transect from Muscat to the south of Wadi Mayh (Figures 2a and 2b). Care was taken to select samples close to the major shear zones recognized in the field [*Searle et al.*, 1994], in order to search for P gaps and contrasts in the P-T evolution. Mineral occurrences are listed in Table 1. Mineral parageneses of the dominantly metapelitic samples are poor, containing mostly phengite, chlorite and in fewer cases additional mineral species among carpholite, chloritoid, pyrophyllite, kaolinite, albite and paragonite.

[17] Petrological and mineralogical constraints are briefly described below (see Figures 3 and 4), from Mascate (e.g., sample R 7.24; Figure 2a) to the southern Wadi Mayh (e.g., sample SF 7.04; Figure 2a), and set back against some of the major tectonic patterns found in the three units. All three units show exhumation-related extensional top to the north patterns and recumbent folding as dominant tectonic features.
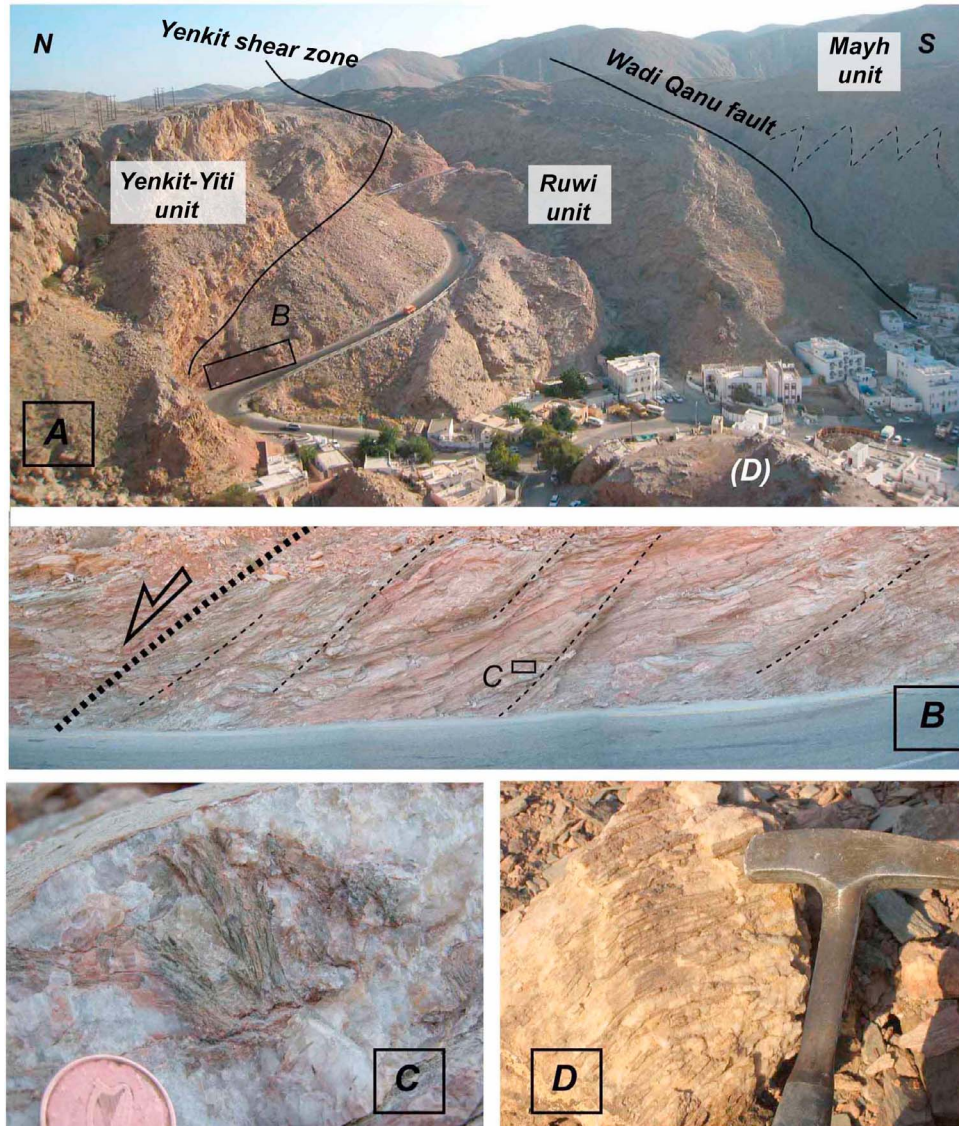
Figure 3. Petrology and structural patterns in the upper Yenkit-Yiti, Ruwi, and Mayh units. (a) Panoramic view (Al Hamriyah, SE Mascate) looking east; the Ruwi unit is bounded by the Yenkit shear zone to the left of the picture and by the Wadi Qanu fault zone to the right. (b) Exhumation-related shear bands with clear top to the north shear criteria, located below the Yenkit shear zone (see box in Figure 3a). (c) Carpholite-bearing quartz-rich boudin preserved within the shear bands (close-up view of area marked in Figure 3b). (d) Fresh carpholite hand specimen from the small hill in Al Hamriyah (see location in Figure 3a). (e, f) Outcrop-scale deformation patterns along the eastern wadi near Yenkit and corresponding sketch. Top to the north extensional shear patterns postdate earlier, recumbent folds probably related to top to the south thickening [e.g., *Michard et al.*, 1994]. (g, h) Exhumation-related top to the north deformation patterns observed opposite outcrop (Figures 3e and 3f). (i) Wadi Mayh, Al Wudya shear zone (location in Figure 2a): top to the north, exhumation-related drag folds. (j) Typical, meter-scale south vergent, reworked folds found within the larger drag folds shown in Figure 3i, which could tentatively be related to earlier top to the south shortening associated with crustal stacking (location is shown in bottom right of Figure 3i). (k) Sheath fold area (southern Wadi Mayh): view eye-to-eye with four stacked sheath folds [*Searle and Alsop*, 2007] best developed within the Permian Saiq Formation. See the truck down the road for scale.
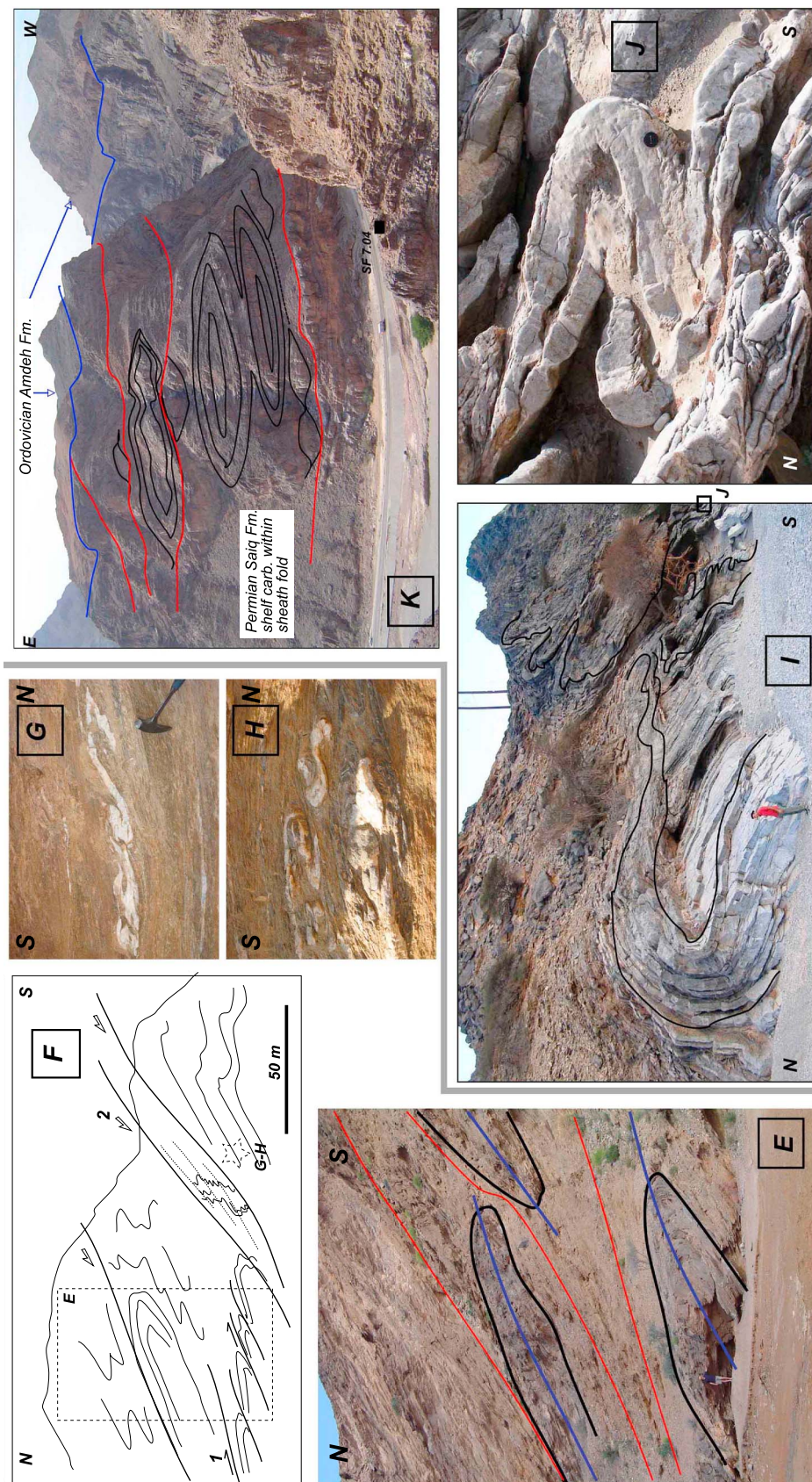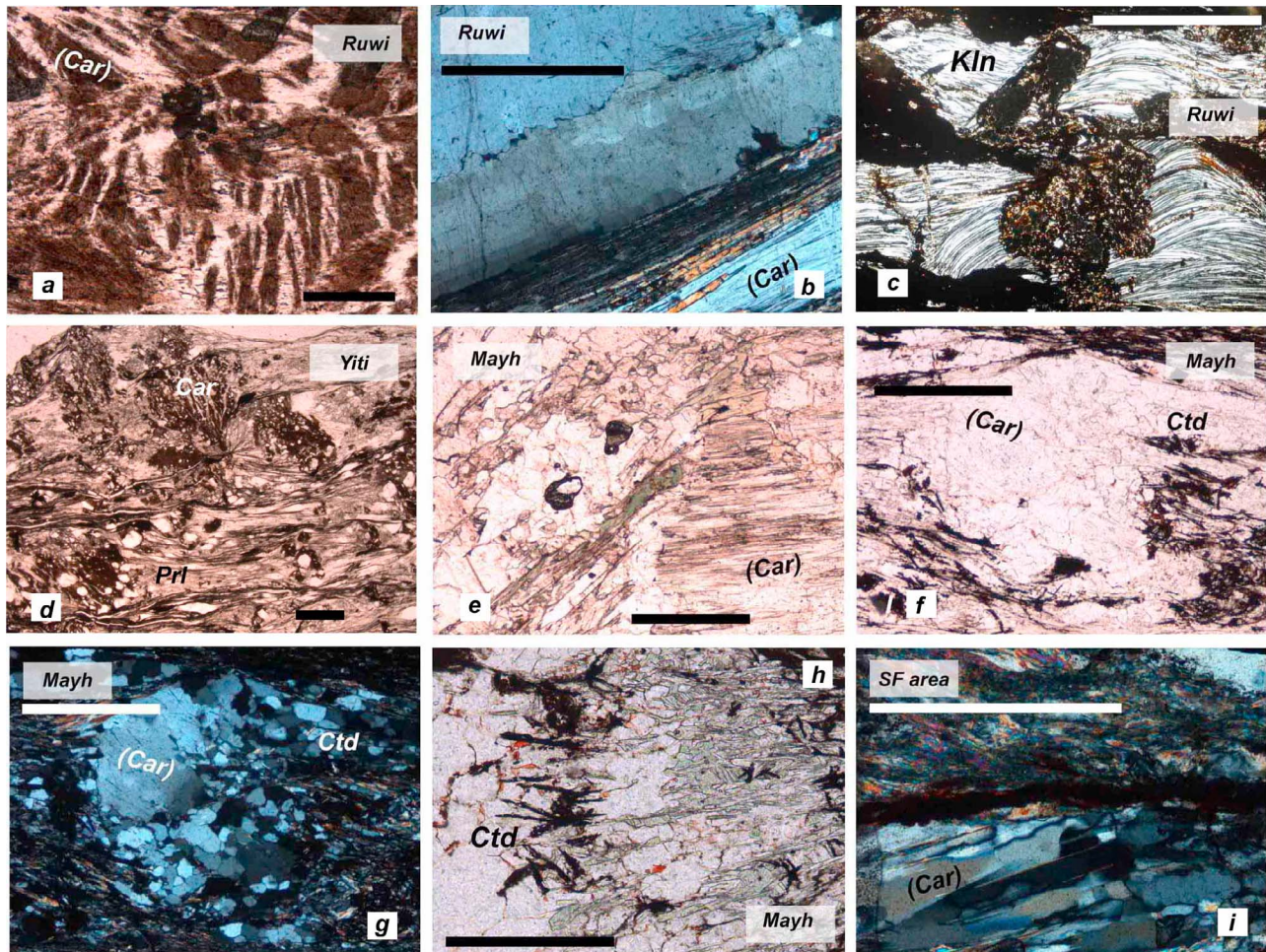
Figure 3. (continued)

Figure 4. Microphotographs from the upper unit samples (plane polarized light and cross-polar light, hereafter PPL and XPL, respectively). See Table 1 for mineral occurrences. Scale bar is 200 μm. (a) Rosette-like aggregates of carpholite, partly pseudomorphed by chlorite and phengite, in the Ruwi unit (sample R 7.07, XPL). (b) Parallel carpholite needles in quartz replaced by chlorite and phengite. Note the more disoriented carpholite crystals, still fresh, in the top right and bottom right of the picture and the irregular grain boundaries suggesting incipient dynamic recrystallization (sample R 7.23, XPL). (c) Kaolinite pressure fringes around opaque minerals and chlorite microcrysts in the Ruwi unit, just above Wadi Qanu fault (sample R. 7.23, XPL). (d) Fresh carpholite crystals and pseudomorphs in highly sheared Jurassic, thinly bedded limestones from the Yenkit-Yiti unit (Yiti beach; sample Y 7.18, XPL). (e) Quartz porphyroblast (to the lower right) hosting carpholite needles. Chlorite and phengite can be recognized outside of quartz, in the smaller grain size, deformed matrix (sample M 5.11). (f, g) Sample M 7.20 (PPL and XPL): quartz porphyroblast still partly hosting carpholite needles on the left-hand side, whereas its second half to the right was dynamically recrystallized into smaller grains, leading to carpholite replacement by chloritoid crystals (small, black rosette-like crystals). (h) The Mayh unit, in addition to carpholite relics (Figures 4e–4g), commonly shows tiny chloritoid crystals that were later pseudomorphed by opaque minerals (larger chloritoid crystals are also shown). (i) Carpholite needles preserved in samples from the SFA. Unfortunately, only equivocal microprobe measurements were obtained on this sample (high noise/signal ratio; sample SF 7.04, XPL). Note the intense shearing attested by quartz grains.

3.1. Ruwi Unit

[18] In the northwest of the study area, in the southeasternmost end of Muscat (Al-Hamriyah), the Ruwi unit is separated from the overlying Yenkit-Yiti unit by the Yenkit shear zone (Figure 3a). This shear zone is a 100–150 m thick zone with distributed shear bands showing clear top-

to-the north shear sense indicators and numerous drag folds (Figures 3a and 3b) suggesting that it is responsible for the unroofing of the Ruwi unit.

[19] Carpholite crystals, testifying to lower-grade blueschist facies conditions, are still fresh in places in the matrix of the Ruwi melange (Figures 3c, 3d, and 4a; as first ob-

Table 2a. Representative Whole-Rock Analyses[a]

	Sample	
	M 5.35	OM 05.30
SiO_2	31.80	68.80
TiO_2	0.49	0.65
Al_2O_3	9.80	13.00
FeO	3.19	4.19
MnO	0.03	0.12
MgO	1.32	1.19
CaO	26.60	2.47
Na_2O	0.38	0.96
K_2O	1.97	2.40
LOI/S	22.77	5.56

[a]LOI/S, loss on ignition (for whole-rock analyses) or analytical sum (for microprobe analyses).

served by [*Goffé et al.*, 1988]), but are best preserved in quartz veins (Figure 4b; sample R 7.24). Note that the presence of carpholite is consistent with the lawsonite occurrences reported in mafic blocks of the Ruwi melange [*El-Shazly and Coleman*, 1990; *El-Shazly*, 1994]. In the thin sections, a few tiny (<100 mm) chloritoid crystals were also observed in apparent equilibrium with carpholite (forming rosette aggregates and bow tie crystals) and chlorite phengite (sample R 7.07; Table 1). Late, syndeformation recrystallization of kaolinite in pressure fringes coeval with the top to the north shear bands are seen around opaque or chlorite porphyroblasts (R 7.23; Figure 4c). Since the Ruwi unit pinches out toward the east, one finds the contact between the Ruwi and Mayh units just a few hundred meters below the Yenkit shear zone (Figure 3a). This limit now corresponds to the brittle Wadi Qanu fault (Figure 3a), which is reworking earlier ductile deformation patterns.

3.2. Yenkit-Yiti Unit

[20] The Yenkit-Yiti unit is made of the Triassic Mahil and Jurassic Sahtan formations unconformably overlain by an Eocene limestone (Figure 2b). Since the lithologies are largely dominated by carbonates, the mineralogical content of the Yenkit-Yiti unit is generally poor and mostly restricted to the high-variant assemblage chlorite and phengite. Carpholite pseudomorphs are nevertheless present in Yiti, together with pyrophyllite (Figure 4d; sample Y 7.18).

[21] Near the base of this unit, one finds a wider deformation zone, distributed over approximately 250–300 m, which corresponds to the eastern extension of the Yenkit shear zone separating the Yenkit-Yiti and the Mayh units. This shear zone contains numerous outcrop-scale recumbent folds (Figures 3e and 3f) showing evidence of significant thickening in the Triassic Mahil Formation as well as in the Permian Saiq Formation (Saiq 2 and 3). Top-to-the south recumbent folding is followed by pervasive boudinage and shear sense indicators, either veins (Figures 3g and 3h) or hectometer-scale shear bands (Figure 3f), suggesting apparent top-to-the north extensional movements. These extensional shear bands evolved into brittle normal faulting.

3.3. Mayh Unit

[22] Deformation patterns are distributed within the Mayh unit, grading from open, kilometer-scale folds to intensely deformed sheath folds to the south of Wadi Mayh (see below). Shear bands and open folds are visible at the meter scale in many places, but a more spectacular concentration of deformation patterns is observed along the northern Wadi Mayh (Figure 3i). They consistently indicate top to the north, exhumation-related shear senses (Figure 3i), with hints of earlier, transposed tight folds likely associated with top to the south folding (Figure 3j).

[23] In the more pelitic layers (e.g., M 7.20; Figure 2a), carpholite pseudomorphs are found as tiny acicular crystals hosted (and protected) in quartz (Figure 4e). These carpholite needles escaped the prograde transformation to chloritoid where hosted in quartz devoid of significant subgrain formation. Indeed, a key observation is that whenever large quartz crystals are dynamically recrystallized into smaller grains (lacking undulate extinction), carpholite is lost (Figures 4f and 4g; for the same process in Ruwi unit, see also Figure 4b). Carpholite was replaced in the matrix by chloritoid, chlorite and phengite. The habitus of chloritoid and carpholite nevertheless suggest that the temperature-dependent carpholite to chloritoid reaction was not strongly overstepped. Chloritoid crystals occur as small rosettes and are often pseudomorphed by opaque minerals (goethite and hematite; Figures 4f and 4h). In the Mayh unit, blue crossitic amphibole is also seen in places (for example, approximately 500 m south of sample M 7.20 [*Searle et al.*, 1994]).

[24] South of Wadi Mayh, the sheath fold area (SFA) (Figures 2a and 2b) shows some of the largest exposed sheath folds on Earth and intense deformation is visible at all scales (Figure 3k) [*Searle and Alsop*, 2007; *Alsop et al.*, 2007]. Figure 4i shows this extreme deformation at the thin section scale, with elongate quartz ribbons in pressure shadows. *Goffé et al.* [1988, Figure 3] report carpholite and pyrophyllite close to this area. Carpholite pseudomorphs are likely in the Wadi Mayh sheath fold area, although this cannot be proven directly. There are typical replacement microtextures and needles resembling those of carpholite (Figure 4i) although, unfortunately, no successful electron microprobe analysis could be made of these very tiny needles. Phyllosilicates are dominantly phengite and pyrophyllite. By contrast, however, exhumation-related kaolinite pressure fringes are found in the north/top of the Mayh unit, just below the Wadi Qanu fault.

[25] Finally, in order to better constrain our tectonic scenario and appraise lateral variations away from the HP Saih Hatat nappe stack, we also attempted to characterize the P-T evolution of the nearby Jebel Akhdar culmination (Figure 1b). No carpholite or pyrophyllite was found in the Jebel Akhdar, however, despite suitable rock protoliths and an intensive search for index mineralogical remnants. This suggests a very strong lateral contrast in the tectonic evolution on either side of the Semail Gap (Figure 1b).

4. P-T Estimates for Uppermost Units

[26] Thirteen samples were studied by electron probe microanalysis (EPMA), seven of which yielded P-T con-

Table 2b. Representative Mineral Analyses[a]

	Carpholite					Chloritoid		Chlorite										Phengite							Pyrophyllite
	Sample 7.24 Analysis ar24	Sample 7.24 Analysis ar25	Sample 7.07 Analysis aq'88	Sample 7.07 Analysis aq'89	Sample 7.07 Analysis aq'90	Sample 7.07 Analysis ba51	Sample m29 Analysis am44	Sample 7.07 Analysis aq'25	Sample 7.07 Analysis aq'31	Sample 7.07 Analysis aq'84	Sample 7.07 Analysis aq'85	Sample 7.20 Analysis aq'19	Sample m29 Analysis am15	Sample m29 Analysis am16	Sample m29 Analysis am36	Sample m11 Analysis am66	Sample m11 Analysis am74	Sample 7.07 Analysis aq'40	Sample 7.07 Analysis aq'48	Sample 7.20 Analysis aq'16	Sample m29 Analysis am49	Sample m29 Analysis am52	Sample m29 Analysis am53	Sample m11 Analysis am62	Sample 7.18 Analysis ar37
Mineral Compositions																									
SiO_2	37.45	38.06	38.12	37.09	37.28	24.43	23.65	24.86	24.74	25.35	24.60	26.11	24.70	24.71	25.40	24.44	24.41	50.09	47.07	48.94	47.74	48.06	47.94	47.65	64.61
TiO_2	0.41	0.22	1.60	1.28	1.25	0.07	0.06	0.04	0.04	0.08	0.04	0.00	0.00	0.03	0.10	0.01	0.04	0.10	0.02	0.17	0.11	0.05	0.15	0.18	0.02
Al_2O_3	30.92	30.83	30.61	30.89	31.01	40.92	38.96	22.81	23.18	23.59	22.70	21.12	21.33	21.14	22.94	21.33	21.15	31.09	34.72	28.34	30.64	30.79	30.70	31.17	28.47
FeO	14.07	14.04	12.80	13.47	14.38	25.74	27.62	28.37	28.01	26.68	26.98	24.84	28.58	31.24	25.53	30.04	32.02	1.91	1.29	3.82	1.94	1.75	1.82	2.12	0.14
MnO	0.24	0.35	0.07	0.31	0.28	0.25	0.14	0.24	0.32	0.11	0.23	0.07	0.07	0.03	0.13	0.11	0.05	0.00	0.00	0.00	0.00	0.02	0.03	0.00	0.00
MgO	4.14	3.76	4.74	4.15	4.18	1.94	1.32	10.73	10.41	10.94	10.66	13.44	11.39	9.85	12.67	9.34	9.06	2.08	1.00	2.19	1.82	1.89	2.01	1.66	0.17
CaO	0.04	0.04	0.05	0.00	0.03	0.00	0.08	0.03	0.00	0.01	0.01	0.04	0.02	0.06	0.13	0.17	0.08	0.07	0.04	0.05	0.07	0.15	0.05	0.08	0.13
Na_2O	0.04	0.00	0.00	0.01	0.01	0.04	0.05	0.01	0.00	0.01	0.00	0.00	0.00	0.00	0.03	0.00	0.03	0.11	1.25	0.22	1.25	0.30	0.30	0.37	0.10
K_2O	0.02	0.00	0.00	0.01	0.11	0.02	0.13	0.01	0.00	0.19	0.05	0.00	0.03	0.00	0.02	0.06	0.05	8.72	8.24	9.75	8.72	8.73	9.21	10.00	0.26
LOI/S	87.32	87.30	87.98	87.21	88.52	93.41	92.01	87.09	86.70	86.96	85.26	85.63	86.12	87.06	86.95	85.49	86.90	94.18	93.62	93.47	92.30	91.73	92.19	93.23	93.89
Structural Formula																									
Si	2.02	2.05	2.02	2.00	1.99	1.00	1.00	2.68	2.67	2.70	2.69	2.80	2.70	2.71	2.69	2.72	2.70	3.32	3.15	3.34	3.26	3.28	3.27	3.24	3.94
Ti	0.02	0.01	0.06	0.05	0.05	0.00	0.00	0.00	0.00	0.01	0.00	0.00	0.00	0.00	0.01	0.00	0.00	0.01	0.00	0.01	0.01	0.00	0.01	0.01	0.00
Al	1.96	1.96	1.92	1.96	1.95	1.98	1.94	2.89	2.95	2.96	2.92	2.67	2.75	2.73	2.87	2.79	2.75	2.43	2.73	2.28	2.47	2.48	2.47	2.50	2.05
Fetot	0.63	0.63	0.57	0.61	0.64	0.88	0.98	2.55	2.53	2.38	2.47	2.23	2.61	2.86	2.26	2.79	2.96	0.11	0.07	0.22	0.11	0.10	0.10	0.12	0.01
Mn	0.01	0.02	0.00	0.01	0.01	0.01	0.01	0.02	0.03	0.01	0.02	0.01	0.01	0.00	0.01	0.01	0.00	0.00	0.00	0.00	0.00	0.00	0.00	0.00	0.00
Mg	0.33	0.30	0.38	0.33	0.33	0.12	0.08	1.72	1.67	1.74	1.74	2.15	1.86	1.61	2.00	1.55	1.49	0.21	0.10	0.22	0.19	0.19	0.20	0.17	0.02
Ca	0.00	0.00	0.00	0.00	0.00	0.00	0.00	0.00	0.00	0.00	0.00	0.00	0.00	0.01	0.01	0.02	0.01	0.00	0.00	0.00	0.01	0.01	0.00	0.01	0.01
Na	0.00	0.00	0.00	0.00	0.00	0.00	0.00	0.00	0.00	0.00	0.00	0.00	0.00	0.00	0.01	0.00	0.01	0.01	0.16	0.03	0.17	0.04	0.04	0.05	0.01
K	0.00	0.00	0.00	0.00	0.01	0.00	0.01	0.00	0.00	0.03	0.01	0.00	0.00	0.00	0.00	0.01	0.01	0.74	0.70	0.85	0.76	0.76	0.80	0.87	0.02
XMg	0.34	0.32	0.40	0.35	0.34	0.12	0.08	0.40	0.40	0.42	0.41	0.49	0.41	0.36	0.47	0.36	0.33	0.66	0.58	0.51	0.63	0.65	0.66	0.58	0.68
nOx	8	8	8	8	8	6	6	14	14	14	14	14	14	14	14	14	14	11	11	11	11	11	11	11	11

[a]Here nOx, number of oxygens on which the structural formula is calculated; XMg, Mg/(Fe + Mg). LOI/S, loss on ignition (for whole-rock analyses) or analytical sum (for microprobe analyses).

straints (see below). In order to derive P-T estimates for these high-variance samples, the multiequilibrium approach of *Berman* [1991] was used as adapted and detailed by *Vidal and Parra* [2000]. Applications of the chlorite-mica-quartz multiequilibrium calculation include *Trotet et al.* [2001], *Vidal et al.* [2001, 2005], *Parra et al.* [2002a], *Ganne et al.* [2003], *Rimmelé et al.* [2004], *Augier et al.* [2005], *Willner et al.* [2004], and *Yamato et al.* [2007]. For the sake of comparison, we also used the independent approach of calculating pseudosections with Perple_X [*Connolly*, 1990, 2009] for representative whole-rock compositions. These P-T estimates are finally compared to the maximum temperatures obtained by *Yamato et al.* [2007] (Figure 2a).

4.1. Whole-Rock and Mineral Chemistry

[27] We selected one representative, carbonate-rich meta-pelitic sample from the Wadi Mayh unit (calc-schist M 5.35) and one from the Permian Saiq Formation of the Hulw unit for comparison (OM 05.30). Major elements analysis was performed at Ecole et Observatoire des Sciences de la Terre in Strasbourg, France, by ICP-AES and ICP-MS (see Table 2a). Analytical procedure is the same as described by *Omrani et al.* [2008]. The Mayh sample shows a significant volatile content (LOI) (Table 2a) consistent with its high carbonate content. These whole-rock compositions were renormalized in the Na_2O-K_2O-FeO-MgO-Al_2O_3-SiO_2-H_2O (NaKFMASH) system, as discussed below.

[28] EPMA was performed using classical analytical conditions for spot analyses (1–2 mm spot size; 15 kV, 10 nA, wavelength-dispersive spectroscopy (WDS) mode), using Fe_2O_3 (Fe), $MnTiO_3$ (Mn, Ti), diopside (Mg, Si), CaF_2 (F), orthoclase (Al, K), anorthite (Ca) and albite (Na) as standards.

[29] Mineral abbreviations used hereafter are Car, Chl, Ctd, Kaol, Qtz, Phg, Prg and Prl for carpholite, chlorite chloritoid, kaolinite, quartz, phengite and pyrophyllite, respectively. Representative analyses are shown in Table 2b. They outline the narrow range of X_{Mg} compositions for both carpholite (0.3–0.38) and chloritoid (0.04–0.12).

[30] By far, however, the most common minerals are phyllosilicates. Paragonite, kaolinite and pyrophyllite, whenever present, are close to their ideal end-member composition. Only phengite and chlorite show significant compositional variations (Figure 5a). Phengite has Si contents mostly in the range 3.09–3.38 per formula unit, with X_{Mg} values of 0.51 to 0.68. Chlorite analyses span a range from $Clin_{62}Ames_{31}Sud_7$ to $Clin_{57}Ames_{22}Sud_{31}$, with X_{Mg} values between 0.31 and 0.49 (Figure 5a).

4.2. TWEEQU Multiequilibrium Thermobarometry

[31] We used the TWEEQU 2.02 software [*Berman*, 1991] and its associated database JUN92 complemented by thermodynamic properties for Mg-amesite, Mg-sudoite, Mg-celadonite for chlorite and phengite solid solution models (25.min and 26.sln) from *Vidal and Parra* [2000]. For phengite and chlorite the assym/25 and VP209 solid solution models are used, respectively. We recall that substitutions are modeled with five end-members in chlorite (clinochlore, Fe- and Mg-amesite, daphnite and Mg-

sudoite), using site-mixing model with symmetric Margules parameters and ideal intersite interactions [*Parra et al.*, 2002b, 2005; *Vidal et al.*, 2005, 2006] and four end-members in dioctahedral K-bearing white mica (Mg- and Fe-celadonite, muscovite, pyrophyllite). With the five chlorite and four dioctahedral phengite end-members defined above, 64 reactions (of which five are independent) can be written in the system Si-Al-Fe-Mg-K-H for a paragenesis comprising phengite, chlorite and quartz in the presence of water. For the divariant Car-Ctd-Chl-Phg paragenesis, eight reactions (i.e., 14 end-members minus 6 chemical components) are independent (out of 732). To evaluate the maximum dispersion of the equilibrium curves, a set of eight independent reactions with the simplest stoichiometric coefficients are highlighted in Figure 5b.

[32] As is the case for other phyllosilicates, the substitution of Al^{3+} for Fe^{3+} also occurs in chlorite, affecting both ideal and nonideal activities of the chlorite end-members. Owing to the difficulty of calculating Fe^{2+}/Fe^{3+} from electron probe microanalysis in such minerals, the Fe^{3+} content was estimated with the method described by *Vidal et al.* [2006]. This method is based on the convergence of the equilibria written among chlorite end-members, quartz and H_2O. The amount of Fe^{3+} in phengite has been estimated with a similar thermodynamic approach using chlorite-phengite equilibria (as in the work by *Vidal et al.* [2006]). The activity of H_2O was considered to equal unity in all calculations. Results of multiequilibrium thermobarometry are shown in Figure 5d.

4.3. Pseudosection Calculations With Perple_X

[33] We used the phase diagram calculation software package Perple_X [*Connolly*, 1990, 2009] (April 2009 version) and the self-consistent thermodynamic database and mineral solution models of *Holland and Powell* [1998] (with the 2002 revision). The compositions of carpholite- or chloritoid-bearing metapelitic layers within Permian cover rocks in NaKFMASH (in wt %, with H_2O in excess) are $Na_2O(0.73)$-$K_2O(3.80)$-$FeO(6.15)$-$MgO(2.54)$-$Al_2O_3(18.88)$-$SiO_2(61.21)$ for the Mayh sample, and Na_2O (0.86)-$K_2O(2.40)$-$FeO(4.04)$-$MgO(1.19)$-$Al_2O_3(13.00)$-$SiO_2(68.80)$ for the one from Hulw. Calcium, which is only hosted by carbonate minerals (calcite or aragonite) or apatite, and titanium, by rutile or titanite, need not be considered here.

[34] Three different pseudosections for Mayh sample M 5.35 are shown in Figure 5c, in which only the divariant Car-Ctd-Chl-Phg-Prg-Qtz-H_2O field is labeled for the sake of clarity. At lower and higher temperatures, one finds the trivariant Car-Chl-Phg-Prg-Qtz-H_2O and Ctd-Chl-Phg-Prg-Qtz-H_2O fields, respectively. The divariant field labeled 1 was calculated with the actual M 5.35 composition, whereas fields labeled 2 and 3 are those obtained when slightly changing the composition of sample M 5.35 to evaluate the influence of variations in the $Na_2O/(Na_2O + K_2O)$ ratio, from 0.16 to 0.25, and in the $MgO/(FeO + MgO)$ ratio, from 0.29 to 0.4. The divariant Car-Ctd-Chl-Phg-Prg-Qtz-H_2O field in sample OM 05.30 (not shown here) is virtually indistinguishable from field 2.

4.4. Overview of the P-T Results

[35] Some of the P-T points, based on multiequilibrium thermobarometry of chlorite-phengite pairs + carpholite and chloritoid, are shown in Figure 5b. These plots readily indicate that (1) peak P-T conditions lie close or within the divariant Car-Ctd-Chl-Phg-Prg-Qtz-H2O field, (2) maxi-mum burial conditions were very similar for the Ruwi and Mayh units and (3) P-T conditions can be determined with a good precision. Results of the calculations are further shown in Figure 5d, where they are differentiated by mineral assemblage and by unit.
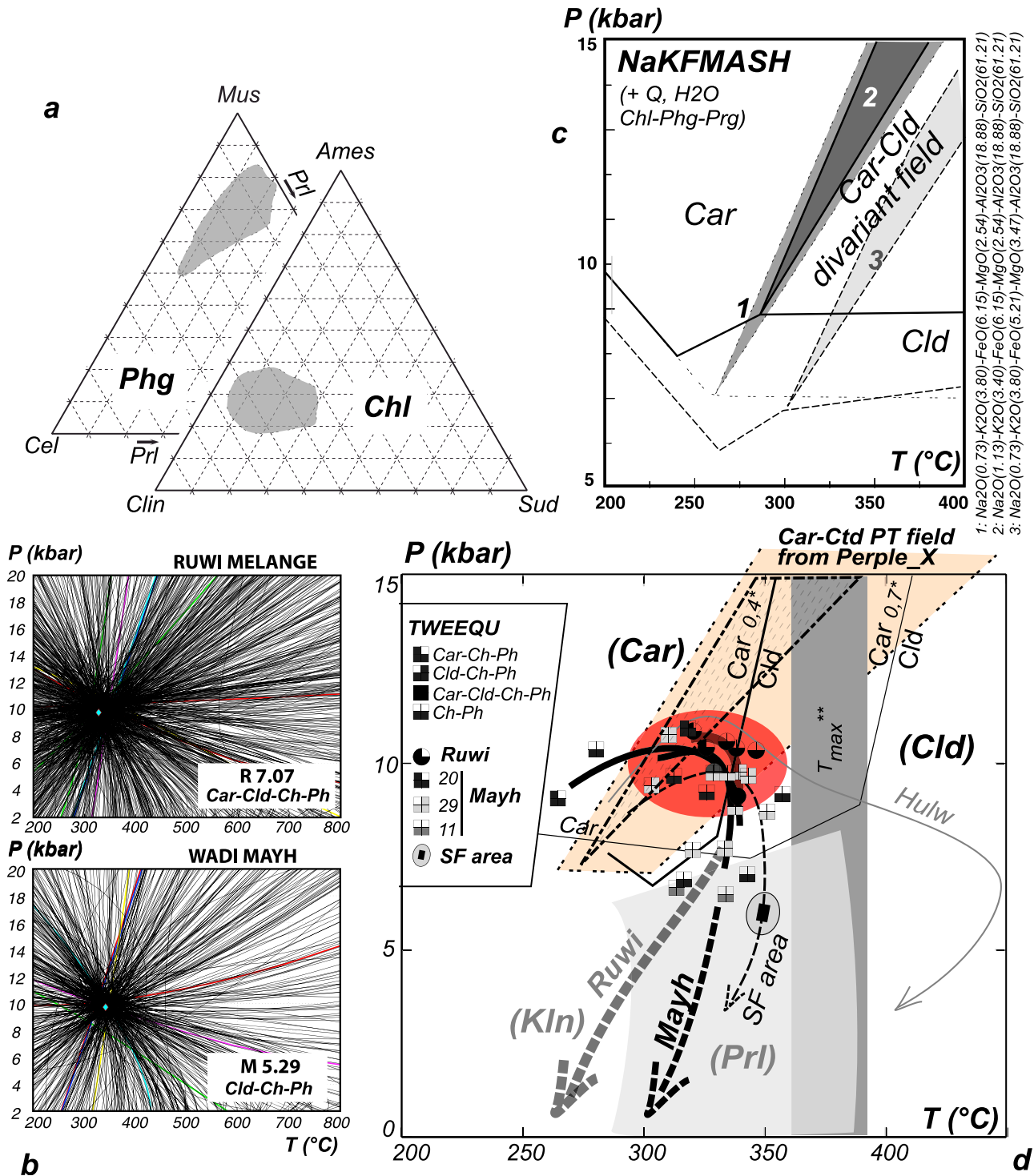
Figure 5

[36] There is indeed a very good agreement between P-T estimates calculated with Car-Chl-Phg assemblages and subsequent Cld-Chl-Phg assemblages, the latter giving T estimates ~20°C–30°C higher on average. Car-Chl-Phg P-T estimates range between 9 and 10.5 kbar at 265°C to 330°C while Cld-Chl-Phg range between 10 and 8.5 kbar at 330°C–340°C. This is consistent with the X_{Mg} value (taken as Mg/Mg + Fe) of carpholite being in the range 0.3–0.37. The position of the Car/Cld divariant reaction for X_{Mg} = 0.4 and 0.7 is also recalled for comparison [Vidal et al., 1992].

[37] With the exception of sample M 5.11, for which a reequilibration step was found at 7 kbar 340°C, most chlorite-phengite pairs (±carpholite and/or chloritoid) yielded peak P-T conditions. In sample R 7.24, for example, where chlorite and phengite are in apparent equilibrium and unequivocally jointly pseudomorph carpholite, no lower-pressure reequilibration P-T estimate could be found, unfortunately. Similarly, no equilibrium P-T value could be found for the Yenkit-Yiti unit. The presence of late pyrophyllite (SFA, southern Mayh unit and Yenkit-Yiti unit) or kaolinite (Ruwi unit and top/north of the Mayh unit) provides additional temperature constraints for the shape of the exhumation paths (Figure 5d).

[38] These multiequilibrium calculations (Figures 5b and 5d) can be compared with the position of the divariant Car-Ctd-Chl-Phg-Prg-Qtz-H_2O field calculated independently with Perple_X (Figure 5c). For Mayh sample M 5.35,

Perple_X yields temperature constraints which are slightly lower (approximately 20°C–30°C; field 1) than those found with TWEEQU, but are in very good agreement from the observed compositions of Car and Ctd (X_{Mg} ~ 0.4 and X_{Mg} ~ 0.1, respectively; Table 2b). According to Perple_X, this field will increase to higher P if there is more Na in the rock (field 2), and it will shift to higher P if the rocks contain more Mg (field 3). Note that more magnesian compositions would shift the Car-Ctd field to higher T and thus completely match the TWEEQU results, but would also result in Car and Ctd compositions richer in Mg than those observed. Overall, the Car-Ctd-Chl-Phg-Prg-Qtz-H_2O field spans the 7–12 kbar depending on element ratio variations (Figure 5d). There is therefore a relatively good agreement between the two methods, suggesting that peak pressure estimates lie in the 9–11 kbar on average.

[39] We finally point out that these P-T estimates for the uppermost Saih Hatat units are just below, and therefore perfectly consistent with, the maximum temperatures obtained for the Mayh unit (approximately 370°C ± 20 [Yamato et al., 2007]; see Figure 2a).

5. Discussion

5.1. HP Metamorphism: Constraints for the Stacking of Cover Units During Continental Subduction

[40] Some major observations can be deduced from the data presented above.

Figure 5. (a) Range of chemical variations found in phengite (Phg) and chlorite (Chl) in the three upper units. End-member abbreviations are as follows: Ames, amesite; Cel, celadonite; Clin, clinochlore; Mus, muscovite; Prl, pyrophyllite; Sud, sudoite. (b) Examples of the graphical representation of the P-T estimates obtained using the TWEEQU multiequilibrium technique with the new software designed by B. Dubacq et al. (manuscript in preparation). P-T estimates are for Ruwi (using carpholite-chloritoid-phengite-chlorite, i.e., eight independent reactions) and Mayh (using chloritoid-phengite-chlorite, i.e., seven independent reactions). We highlighted a set of independent equilibria in each of the panels (the simplest ones, i.e., those with the smallest stoichiometric coefficients) in order give an idea of the maximal dispersion of the curves. For the Ruwi example, these are −2 Mgcarpholite + alpha-quartz + sudoite (red), −Mgcarpholite + alpha-quartz + H_2O + Mg-chloritoid (green, steepest slope), −5 Mg-celadonite + clinochlore − daphnite + 5 Fe-celadonite (blue), −Mg-celadonite + clinochlore − Mg-amesite + muscovite (yellow), −4 Mg-celadonite − Fe-amesite + 4 Fe-celadonite + Mg-amesite (cyan); Mg-celadonite − Fe-celadonite − Mg-chloritoid + Fe-chloritoid (magenta), −Mgcarpholite + Mg-celadonite − 7 alpha-quartz − muscovite + 2 Pyrophyllite (red, negative slope), and −3 Mgcarpholite + 5 alpha-quartz − clinochlore + 2 Mg-amesite + 2 H_2O (green). These plots demonstrate that (1) maximum burial conditions were very similar for the Ruwi and Mayh units and (2) P-T conditions can be determined with a good precision. Corresponding analyses are given in Table 2b. See text for further details. (c) Position of the divariant Car-Ctd-Chl-Phg-Prg-Qtz-H_2O field (gray overlay) for three pseudosections calculated with excess H_2O with Perple_X [Connolly, 1990, 2009] and the self-consistent thermodynamic database and mineral solution models of Holland and Powell [1998]. Whole-rock compositions (in wt %) are given to the right of the panel. For the sake of clarity, the largely temperature-dependent X_{Mg} isopleths of carpholite and chloritoid are not shown here but match very well the observed compositions for fields 1 and 2. See text for details. (d) Summary of the P-T results obtained in this study. The position of the carpholite-chloritoid (Car/Cld) divariant reaction for X_{Mg} = 0.4 and 0.7 is also recalled for comparison [Vidal et al., 1992]. P-T estimates by multiequilibrium calculations are differentiated by mineral assemblage and by unit (symbols to the left). The P-T range for the divariant Car-Ctd-Chl-Phg-Prg-Qtz-H_2O field calculated independently with Perple_X is shown (see also Figure 5c). The hatched field with a thick contour, calculated with Perple_X, best fits carpholite and chloritoid compositions measured in the Mayh unit. There is a relatively good agreement between the multiequilibrium technique and minimization with Perple_X, suggesting that peak pressure estimates lie in the 9–11 kbar on average. Maximum temperatures for these upper units (T_{max}** [Yamato et al., 2007], dark gray vertical field) are consistent with our P-T estimates. There is a slight temperature difference on exhumation between the kaolinite-bearing Ruwi unit and the pyrophyllite-bearing Mayh and Yenkit-Yiti units. Note, finally, the striking similarity of peak P-T conditions and the distinctive warmer excursion obtained for the Hulw unit by Yamato et al. [2007].
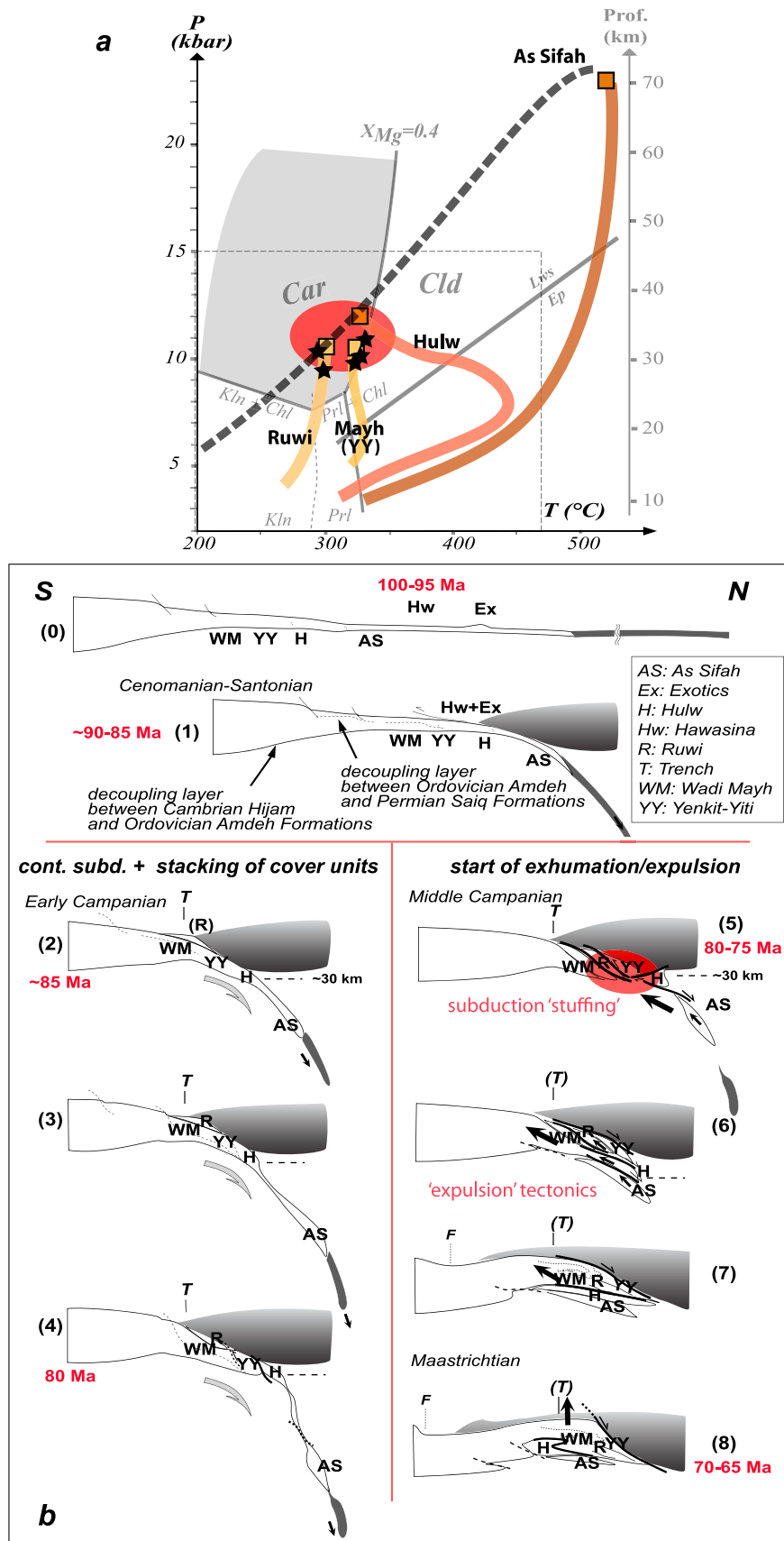
Figure 6

[41] 1. Pressure estimates lie uniformly in the range 9–11 kbar in the upper plate Ruwi and Mayh units, and very likely in the carpholite-bearing Yenkit-Yiti unit (Figure 5c). These estimates are greater than those of *El-Shazly* [1994, 1995] (3–6 and 6–9 kbar for Ruwi and Mayh, respectively) and somewhat greater than those of *Goffé et al.* [1988] (~8 kbar). Contrary to the latter, however, mineralogical evidence supports a clockwise P-T evolution (as for lower plate rocks [*El-Shazly et al.*, 1990; *Yamato et al.*, 2007]).

[42] 2. These identical mineralogical evolution and pressure values in these units discount earlier claims of a down-section gradient in pressure [*El-Shazly*, 1994].

[43] 3. No pressure gap exists across the so-called upper plate/lower plate (i.e., between the Mayh and Hulw units), as shown in Figure 6a. The Hulw unit, however, had a significantly warmer exhumation path (Figure 6a).

[44] 4. Return paths for the upper units differ slightly in terms of temperature, with a warmer exhumation on average for the pyrophyllite-bearing Mayh unit (except in the north, where kaolinite is found) than for the kaolinite-bearing Ruwi unit (Figure 5d). We note that south of the Al Wudya shear zone (Figures 2a and 2b), temperature estimates deduced from multiequilibrium thermobarometry (i.e., 340°C ± 20°) fit with maximum temperatures inferred from the Raman spectroscopy of carbonaceous material (~370°C ± 30 [*Yamato et al.*, 2007]).

[45] 5. As underlined by earlier workers [*Michard et al.*, 1994; *Searle et al.*, 1994, 2004; *Miller et al.*, 2002, *Jolivet et al.*, 1998; *Warren and Miller*, 2007; *Yamato et al.*, 2007; *Chauvet et al.*, 2009], deformation patterns on the shear zones described above indicate dominantly top to the north extensional patterns overprinting and postdating evidence of earlier southward directed thickening.

[46] These observations have the following implications.

[47] 1. The Ruwi, Yenkit-Yiti, and Mayh units, as well as the Hulw unit, all reached the same depth range. This demonstrates the stacking of Permian and Triassic, predominantly calcareous units at the same depths ~30–35 km in the subduction zone. This also suggests that continental subduction processes were efficient enough to drag cover rocks at similar depths for a significant amount of time (circa 5 Ma, between 80 and 75 Ma and 75–70 Ma [*El-Shazly and Lanphere*, 1992; *Miller et al.*, 1999]).

[48] 2. By comparison with the upper units, the Hulw unit, generally considered a more distal unit than the Mayh unit (Figure 1c), shows a significantly warmer temperature excursion: this could tentatively be related to a longer storage of the Hulw unit at ~30–35 km depth. Alternatively, this warmer excursion could relate to its juxtaposition with the As Sifah eclogites (Figure 6a) or with a crustal unit still hidden below.

[49] 3. Shear bands show very little pressure offset and therefore minimal amounts of vertical exhumation but possibly considerable horizontal translation.

[50] 4. This study emphasizes the importance of mechanical decoupling between cover units and basement ones [*Searle et al.*, 2004] and sheds light on the fate of cover units during continental subduction. Despite the fact that all these units, from the Hulw to the Ruwi unit, were subducted to similar depths (i.e., ~30–35 km), the formations and thicknesses involved differ somewhat: Ordovician Amdeh Formation or younger (Hulw unit), Permian Saiq Formation or younger (Mayh unit), Triassic Mahil Formation or younger (Yenkit-Yiti unit), and Cretaceous (Ruwi unit). This may relate to changes with time of the mechanical decoupling horizon (e.g., between the Amdeh and Saiq formations to form the Mayh unit and between the Saiq and Mahil formations for the Yenkit-Yiti unit) and to the progressive choking of the subduction zone during continental subduction (and obduction). Permian and younger formations were in any case scrapped off the subducting continental margin.

5.2. Proposed Model for the Exhumation of Oman HP Rocks

[51] These new results, together with the geological mapping, structural, thermobarometric and geochronological data from Oman allow us to propose a model for the exhumation of HP rocks beneath the obducted Semail ophiolite during the Late Cretaceous (Figures 6a and 6b). This model involves rapid subduction of the leading margin of the Arabian continental crust during the later stages of ophiolite obduction, eclogite facies metamorphism, subduction failure during choking of the subduction zone by the arrival of thick shelf carbonates, and rapid exhumation

Figure 6. (a) Our P-T estimates (Figure 5d) are set back against the other well-constrained P-T estimates for the Saih Hatat nappe stack [*Searle et al.*, 1994; *Warren and Waters*, 2006; *Yamato et al.*, 2007] (see Figure 2b for their respective position in the cross section). Overall, these P-T estimates line up on a common P-T gradient yet show contrasting P-T exhumation paths. (b) Geodynamic sketch depicting the tectonic evolution of the major units of the Saih Hatat window, with emphasis on the crustal stacking (steps 4 and 5) and tectonic expulsion of cover-scale imbricates (after step 5). Our P-T estimates and constraints on exhumation paths, combined with the results of previous geological mapping, structural, thermobarometric, and geochronological data from Oman, allow us to propose a model for the exhumation of HP continental rocks subducted beneath the Semail ophiolite. This model involves rapid subduction of the leading margin of the Arabian continental crust during the later stages of ophiolite obduction, eclogite facies metamorphism, subduction failure during chocking of the subduction zone by the arrival of thick shelf carbonates, and rapid exhumation during channelized return flow beneath the ophiolite along the same subduction zone. Abbreviations for units are AS, As Sifah; H, Hulw; R, Ruwi; WM, Wadi Mayh; and YY, Yenkit-Yiti units; Ex, Exotics; Hw, Hawasina. F, location of the flexural foreland; T, position of the subduction trench. The so-called upper plate–lower plate discontinuity is shown, in step 8, as a thick folded line separating the Wadi Mayh and Hulw units. See text for further details.

during channelized return flow beneath the ophiolite along the same subduction zone.

[52] Our proposed model for the formation, preservation and exhumation of the Oman HP rocks involves four main "stages" within a continuum of deformation associated with the emplacement of the Semail ophiolite (steps 0–8; Figure 6b).

[53] 1. Stage 1 (Cenomanian to Santonian; step 1; Figure 6b) includes obduction of the Semail ophiolite, plus the underlying Haybi and Hawasina thrust sheets from NE to SW over the depressed northern continental margin of Arabia by up to 400–450 km [*Glennie et al.*, 1973, 1974; *Searle*, 1985, 2007]. Early NE directed subduction of old, mainly Triassic oceanic crust and sedimentary cover formed the ~10–12 kbar garnet + clinopyroxene amphibolites along the high-temperature intermediate pressure metamorphic sole (Figure 1b) [*Searle and Malpas*, 1980, 1982; *Gnos*, 1998; *Searle and Cox*, 1999, 2002]. Deep oceanic subduction beneath the ophiolite evolved with time and space into a thin-skinned thrust belt when the oceanic thrust sheets were emplaced onto the continental margin.

[54] 2. In stage 2 (Early Campanian; steps 2–4; Figure 6b), during the later stages of ophiolite emplacement, the leading NE continental margin was dragged down the subduction zone. The Permian Saiq Formation carbonates with their basaltic sills and flows were subducted to depths of ~80–90 km (20–23 kbar [*Searle et al.*, 1994, 2004; *Warren and Waters*, 2006]). Higher crustal levels (Triassic-Cretaceous shelf carbonates and the allochthonous units above) and possibly somewhat thicker parts of the more proximal margin (Hulw unit) were not subducted to these depths, so we infer a major detachment corresponding to the Ash Sheik–Diqdah shear zone [*Searle et al.*, 1994, 2004; *Yamato et al.*, 2007] separating these levels. Peak eclogite metamorphism has been dated at 78.95 ± 0.13 Ma from U-Pb zircon dating [*Warren et al.*, 2003, 2005]. Recumbent folding and extreme ductile shearing accompanied prograde HP metamorphism and deep crustal subduction.

[55] 3. In stage 3 (Middle Campanian; steps 5–7, Figure 6b), exhumation of the As Sifah eclogites occurred immediately following peak HP metamorphism by return flow beneath the Ash Sheik–Diqdah shear zone and passive roof fault. NNE facing folds were formed by SSW directed footwall exhumation of the HP rocks. Peak metamorphism in the Hulw unit was 10–12 kbar and 250°C–300°C, before later reequilibration at 8–10 kbar and 450°C [*Yamato et al.*, 2007]. The Ruwi, Yenkit-Yiti and Mayh units all reached similar depths as the Hulw unit. Sheath folds from microscale to macroscale [*Searle and Alsop*, 2007] likely formed at carpholite grade pressures (>8–10 kbar) and depths of 25–30 km. Carpholite-bearing assemblages in the Hulw, Mayh, Yenkit-Yiti and Ruwi units show that all formed at similar high pressures between 8 and 10 kbar. Little or no P-T gaps occur across the bounding shear zones showing that although strain was high, and folding and shearing was intense, little offset or throw occurred along them. These depths of ~30–35 km are probably not

fortuitous since they correspond to the depths at which material is underplated in subduction zones (e.g., Andes [*ANCORP Working Group*, 2003]; Neotethys [*Monié and Agard*, 2009]). The warmer excursion of the Hulw unit could be related to a longer storage of this unit at depths (steps 4–6; Figure 6b). ^{40}Ar-^{39}Ar ages from phengites in the Mayh unit span 80–70 Ma and reflect cooling during exhumation [*Miller et al.*, 1999, 2002].

[56] 4. In stage 4 (Maastrichtian-Paleocene; step 8; Figure 6b), the final stage of exhumation was accomplished along brittle faults that cut the ductile shear zones [*Mann et al.*, 1990; *Fournier et al.*, 2006]. The highest and youngest of these faults is the Wadi Kabir fault that cuts the Yenkit ductile shear zone and downthrows the ophiolite (Figure 2a). This fault remained active into the Late Paleocene as Paleocene Umm er Radhuma limestones have been downthrown by 100 m to the north in the Al Bustan region east of Muscat [*Searle et al.*, 2004].

6. Conclusions

[57] Here we highlight the main conclusions.

[58] 1. Peak P-T estimates determined by two independent methods (TWEEQU and Perple_X) indicate that burial conditions were similar for the Mayh, Yenkit-Yiti and Ruwi upper units. All contain carpholite and/or chloritoid crystals indicating that these formed at high pressure (>8–10 kbar) but low temperature (<330°C). Likewise, the megasheath fold exposed along Wadi Mayh [*Searle and Alsop*, 2007] formed at carpholite grade pressure and depths >25–30 km.

[59] 2. These upper units formed at similar intermediate high pressures (~10 kbar) as the Hulw unit rocks. The Hulw shear zone (upper plate–lower plate discontinuity) and the Yenkit shear zones are thus both major ductile shear zones showing minimal amounts of vertical exhumation but possibly considerable horizontal translation. The excursion of the Hulw unit toward higher temperature during exhumation [*Yamato et al.*, 2007] could suggest longer storage at depth.

[60] 3. A major pressure jump exists between the deepest structural level As Sifah eclogites (20–21 kbar, 80–90 km depth) and the structurally overlying units (Hulw, Mayh, Yenkit-Yiti and Ruwi units). The Hulw unit rocks never reached these pressures and depths so they cannot be included in the same structural package as the As Sifah eclogites [*Gray et al.*, 2004b, 2005; *Warren and Miller*, 2007]. The term upper plate–lower plate discontinuity [*Gregory et al.*, 1998; *Miller et al.*, 1998, 1999, 2002; *Gray et al.*, 2000; *Warren and Miller*, 2007] should be discarded; neither have plate-like characteristics and both are deformed internally by intense ductile shearing. This major contact nevertheless separates continental margin units that were deeply subducted (As Sifah) or underplated (Hulw) from those (Ruwi, Yenkit-Yiti, and Mayh) which were later stacked at depths ~30 km and choked the subduction zone before the exhumation of all HP units.

[61] 4. Our study provides a record of how continental material (thick platform shelf carbonates) progressively

choked a subduction zone. Noteworthily, exhumation of HP eclogites and blueschists in NE Oman was accomplished by extreme ductile shearing during bottom-to-SSW exhumation (or "expulsion") beneath passive roof faults, resulting in the thrusting of footwall rocks toward the continental margin [*Searle et al.*, 1994, 2004; *El-Shazly et al.*, 2001; *Breton et al.*, 2004; *Yamato et al.*, 2007], not away from it [*Gregory et al.*, 1998; *Miller et al.*, 1999, 2002; *Gray et al.*, 2004a, 2004b].

References

Agard, P., L. Jolivet, B. Vrielinck, E. Burov, and P. Monié (2007), Plate acceleration: The obduction trigger?, *Earth Planet. Sci. Lett.*, *258*, 428–441, doi:10.1016/j.epsl.2007.04.002.

Alsop, G. I., R. E. Holdsworth, and K. J. W. McCaffrey (2007), Scale invariant sheath folds in salt, sediments and shear zones, *J. Struct. Geol.*, *29*, 1585–1604, doi:10.1016/j.jsg.2007.07.012.

ANCORP Working Group (2003), Seismic imaging of a convergent continental margin and plateau in the central Andes (Andean Continental Research Project 1996 (ANCORP'96)), *J. Geophys. Res.*, *108*(B7), 2328, doi:10.1029/2002JB001771.

Augier, R., P. Agard, P. Monié, L. Jolivet, C. Robin, and G. Booth-Rea (2005), Exhumation, doming and slab retreat in the Betic Cordillera (SE Spain): In situ ^{40}Ar/^{39}Ar ages and *P-T-d-t* paths for the Nevado-Filabride complex, *J. Metamorph. Geol.*, *23*, 357–381, doi:10.1111/j.1525-1314.2005.00581.x.

Baldwin, S. L., B. D. Monteleone, L. E. Webb, P. G. Fitzgerald, M. Grove, and E. June Hill (2004), Pliocene eclogite exhumation at plate tectonic rates in eastern Papua New Guinea, *Nature*, *431*, 263–267, doi:10.1038/nature02846.

Béchennec, F., J. Le Métour, D. Rabu, C. Bourdillon-Jeudy-de-Gricssac, P. De Wever, M. Beurrier, and M. Villey (1990), The Hawasina Nappes: Stratigraphy, palaeogeography and structural evolution of a fragment of the south-Tethyan passive continental margin, in *The Geology and Tectonics of the Oman Region*, edited by A. H. F. Robertson, M. P. Searle, and A. C. Ries, *Geol. Soc. Spec. Publ.*, *49*, 213–224.

Berman, R. G. (1991), Thermobarometry using multi-equilibrium calculations: A new technique, with petrological applications, *Can. Mineral.*, *29*, 833–855.

Boudier, F., G. Ceuleneer, and A. Nicolas (1988), Shear zones, thrusts and related magmatism in the Oman ophiolite: Initiation of thrusting on an oceanic ridge, *Tectonophysics*, *151*, 275–296, doi:10.1016/0040-1951(88)90249-1.

Breton, J.-P., F. Béchennec, J. Le Métour, L. Moen-Maurel, and P. Razin (2004), Eoalpine (Cretaceous) evolution of the Oman Tethyan continental margin: Insights from a structural field study in Jabal Akhdar (Oman Mountains), *GeoArabia*, *9*, 1–18.

Chauvet, F. (2007), *La Marge Continentale sud-Téthysienne en Oman: Structure et Volcanisme au Permien et au Trias*, 420 pp., Univ. de Grenoble, Grenoble, France.

Chauvet, F., T. Dumont, and C. Basile (2009), Structures and timing of Permian rifting in the central Oman Mountains (Saih Hatat), *Tectonophysics*, *475*, 563–574, doi:10.1016/j.tecto.2009.07.008.

Chemenda, A. I., M. Mattauer, J. Malavieille, and A. N. Bokun (1995), A mechanism for syn-collision rock exhumation and associated normal faulting: Results from physical modelling, *Earth Planet. Sci. Lett.*, *132*, 225–232, doi:10.1016/0012-821X(95)00042-B.

Chemenda, A. I., M. Mattauer, and A. N. Bokun (1996), Continental subduction and a mechanism for exhumation of high-pressure metamorphic rocks: New modelling, field data from Oman, *Earth Planet. Sci. Lett.*, *143*, 173–182, doi:10.1016/0012-821X(96)00123-9.

Chopin, C. (1984), Coesite and pure pyrope in high-grade blueschists of the Western Alps: A first record

and some consequences, *Contrib. Mineral. Petrol.*, *86*, 107–118, doi:10.1007/BF00381838.

Chopin, C., C. Henry, and A. Michard (1991), Geology and petrology of the coesite-bearing terrain, Dora Maira massif, Western Alps, *Eur. J. Mineral.*, *3*, 263–291.

Coleman, R. G. (1971), Plate tectonic emplacement of upper mantle peridotites along continental edges, *J. Geophys. Res.*, *76*, 1212–1222, doi:10.1029/JB076i005p01212.

Coleman, R. G. (1981), Tectonic setting for ophiolite obduction in Oman, *J. Geophys. Res.*, *86*, 2497–2508, doi:10.1029/JB086iB04p02497.

Connolly, J. A. D. (1990), Multivariable phase diagrams: An algorithm based on generalized thermodynamics, *Am. J. Sci.*, *290*, 666–718.

Connolly, J. A. D. (2009), The geodynamic equation of state: What and how, *Geochem. Geophys. Geosyst.*, *10*, Q10014, doi:10.1029/2009GC002540.

Duchêne, S., J.-M. Lardeaux, and F. Albarède (1997), Exhumation of eclogites: Insights from depth-time path analysis, *Tectonophysics*, *280*, 125–140, doi:10.1016/S0040-1951(97)00143-1.

El-Shazly, A. K. (1994), Petrology of lawsonite-, pumpellyite- and sodic amphibole-bearing metabasites from north-east Oman, *J. Metamorph. Geol.*, *12*, 23–48, doi:10.1111/j.1525-1314.1994.tb00002.x.

El-Shazly, A. K. (1995), Petrology of Fe-Mg-carpholite-bearing metasediments from NE Oman, *J. Metamorph. Geol.*, *13*, 379–396, doi:10.1111/j.1525-1314.1995.tb00227.x.

El-Shazly, A. K., and R. G. Coleman (1990), Metamorphism in the Oman Mountains in relation to the ophiolite emplacement, in *The Geology and Tectonics of the Oman Region*, edited by A. H. F. Robertson, M. P. Searle, and A. Ries, *Geol. Soc. Spec. Publ.*, *49*, 475–495.

El-Shazly, A. K., and M. A. Lanphere (1992), Two high pressure metamorphic events in NE Oman: Evidence from ^{40}Ar/^{39}Ar dating and petrological data, *J. Geol.*, *100*, 731–751, doi:10.1086/629625.

El-Shazly, A. K., R. G. Coleman, and J. G. Liou (1990), Eclogites and blueschists from northeastern Oman: Petrology and *P-T* evolution, *J. Petrol.*, *31*, 629–666.

El-Shazly, A. K., M. A. Worthing, and J. G. Liou (1997), Interlayered eclogites, blueschists and epidote amphibolites from NE Oman: A record of protolith compositional control and limited fluid infiltration, *J. Petrol.*, *38*, 1461–1487, doi:10.1093/petrology/38.11.1461.

El-Shazly, A. K., M. Bröcker, B. Hacker, and A. Calvert (2001), Formation and exhumation of blueschists and eclogites from NE Oman: New perspectives from Rb-Sr and ^{40}Ar/^{39}Ar dating, *J. Metamorph. Geol.*, *19*, 233–248, doi:10.1046/j.1525-1314.2001.00309.x.

Ernst, W. G. (2001), Subduction, ultrahigh-pressure metamorphism, and regurgitation of buoyant crustal slices—Implications for arcs and continental growth, *Phys. Earth Planet. Inter.*, *127*, 253–275, doi:10.1016/S0031-9201(01)00231-X.

Fournier, M., C. Lepvrier, P. Razin, and L. Jolivet (2006), Post-obduction extension in the Oman Mountains and subsequent compression, *GeoArabia*, *4*, 17–40.

Ganne, J., F. Bussy, and O. Vidal (2003), Multi-stage garnet in the internal Briançonnais basement (Ambin Massif, Savoy): New petrological con-

straints on the blueschist-facies metamorphism in the Western Alps and tectonic implications, *J. Petrol.*, *44*, 1281–1308, doi:10.1093/petrology/44.7.1281.

Glennie, K. W., M. G. Boeuf, M. H. W. Hughes-Clarke, M. Moody-Stuart, W. F. Pilaar, and B. M. Reinhardt (1973), Late Cretaceous nappes in the Oman mountains and their geologic evolution, *Am. Assoc. Pet. Geol. Bull.*, *57*, 5–27.

Glennie, K. W., M. G. Boeuf, M. H. W. Hughes-Clarke, M. Moody-Stuart, W. F. Pilaar, and B. M. Reinhardt (1974), *Geology of the Oman Mountains*, *Verh. K. Ned. Geol. Mijnbouwkg. Genoot.*, *31*, 423 pp.

Gnos, E. (1998), Peak metamorphic conditions in garnet amphibolites beneath the Semail ophiolite: Implications for an inverted pressure gradient, *Int. Geol. Rev.*, *40*, 281–304, doi:10.1080/00206819809465210.

Goffé, B., A. Michard, J. R. Kienast, and O. Le Mer (1988), A case of obduction-related high-pressure, low-temperature metamorphism in upper crustal nappes, Arabian continental margin, Oman: *P-T* paths and kinematic interpretation, *Tectonophysics*, *151*, 363–386, doi:10.1016/0040-1951(88)90253-3.

Gray, D. R., and R. T. Gregory (2003), Ophiolite obduction and the Samail ophiolite: The behaviour of the underlying margin, in *Ophiolites and Earth History*, edited by Y. Dilek and P. T. Robinson, *Geol. Soc. Spec. Publ.*, *218*, 449–466.

Gray, D. R., R. T. Gregory, and J. M. Miller (2000), A new structural profile along the Muscat-Ibra transect, Oman: Implications for the emplacement of the Samail ophiolite, in *Ophiolites and Oceanic Crust: New Insights From Field Studies and the Ocean Drilling Program*, edited by Y. Dilek et al., *Geol. Soc. Am. Spec. Pap.*, *349*, 513–523.

Gray, D. R., M. Hand, J. Mawby, R. A. Armstrong, J. M. Miller, and R. T. Gregory (2004a), Sm-Nd and zircon U-Pb ages from garnet-bearing eclogites, NE Oman: Constraints on high-P metamorphism, *Earth Planet. Sci. Lett.*, *222*, 407–422, doi:10.1016/j.epsl.2004.03.016.

Gray, D. R., J. M. Miller, D. A. Foster, and R. T. Gregory (2004b), Transition from subduction- to exhumation-related fabrics in glaucophane-bearing eclogites, Oman: Evidence from relative fabric chronology and ^{40}Ar/^{39}Ar ages, *Tectonophysics*, *389*, 35–64, doi:10.1016/j.tecto.2004.06.016.

Gray, D. R., R. T. Gregory, and J. M. Miller (2005), Comment on "Structural evolution, metamorphism and restoration of the Arabian continental margin, Saih Hatat region, Oman Mountains," *J. Struct. Geol.*, *27*, 371–374, doi:10.1016/j.jsg.2004.07.002.

Gregory, R. T., D. R. Gray, and J. M. Miller (1998), Tectonics of the Arabian margin associated with the formation and exhumation of high-pressure rocks, Sultanate of Oman, *Tectonics*, *17*, 657–670, doi:10.1029/98TC02206.

Hacker, B. R., L. Ratschbacher, L. Webb, and D. Shuwen (1995), What brought them up? Exhumation of the Dabie Shan ultrahigh-pressure rocks, *Geology*, *23*, 743–746, doi:10.1130/0091-7613(1995)023<0743:WBTUEO>2.3.CO;2.

Hacker, B. R., J. L. Mosenfelder, and E. Gnos (1996), Rapid emplacement of the Oman ophiolite: Thermal and geochronologic constraints, *Tectonics*, *15*, 1230–1247, doi:10.1029/96TC01973.

Hacker, B. R., A. Calverta, R. Y. Zhang, W. G. Ernst, and J. G. Liou (2003), Ultrarapid exhuma-

tion of ultrahigh-pressure diamond-bearing meta-sedimentary rocks of the Kokchetav Massif, Kazakhstan?, *Lithos*, *70*, 61–75, doi:10.1016/S0024-4937(03)00092-6.

Hacker, B. R., T. B. Andersen, S. Johnston, A. R. C. Kylander-Clark, E. M. Peterman, E. O. Walsh, and D. Young (2010), High-temperature deformation during continental-margin subduction and exhumation: The ultrahigh-pressure Western Gneiss Region of Norway, *Tectonophysics*, *480*, 149–171, doi:10.1016/j.tecto.2009.08.012.

Hermann, J., D. Rubatto, A. Korsakov, and V. S. Shatsky (2001), Multiple zircon growth during fast exhumation of diamondiferous, deeply subducted continental crust (Kokchetav Massif, Kazakhstan), *Contrib. Mineral. Petrol.*, *141*, 66–82.

Holland, T. J. B., and R. Powell (1998), An internally consistent thermodynamic data set for phases of petrological interest, *J. Metamorph. Geol.*, *16*, 309–343, doi:10.1111/j.1525-1314.1998.00140.x.

Jolivet, L., B. Goffé, R. Bousquet, R. Oberhänsli, and A. Michard (1998), Detachments in high-pressure mountain belts, Tethyan examples, *Earth Planet. Sci. Lett.*, *160*, 31–47, doi:10.1016/S0012-821X(98)00069-X.

Jolivet, L., H. Raimbourg, L. Labrousse, D. Avigad, Y. Leroy, H. Austrheim, and T. B. Andersen (2005), Softening trigerred by eclogitization, the first step toward exhumation during continental subduction, *Earth Planet. Sci. Lett.*, *237*, 532–547, doi:10.1016/j.epsl.2005.06.047.

Kylander-Clark, A. R. C., B. R. Hacker, and J. M. Mattinson (2008), Slow exhumation of UHP terranes: Titanite and rutile ages of the Western Gneiss Region, Norway, *Earth Planet. Sci. Lett.*, *272*, 531–540, doi:10.1016/j.epsl.2008.05.019.

Le Métour, J., M. Villey, and X. de Gramont (1986a), Geological map of Quryat, sheet NF 40-4D, Minist. of Pet. and Miner., Muscat, Oman.

Le Métour, J., M. Villey, and X. de Gramont (1986b), Geological map of Masqat, sheet NF 40-4A, Minist. of Pet. and Miner., Muscat, Oman.

Lippard, S. J. (1983), Cretaceous high pressure metamorphism in NE Oman and its relationship to subduction and ophiolite nappe emplacement, *J. Geol. Soc.*, *140*, 97–104, doi:10.1144/gsjgs.140.1.0097.

Liu, F. L., A. Gerdes, J. G. Liou, H. M. Xue, and F. H. Liang (2006), SHRIMP U-Pb zircon dating from Sulu-Dabie dolomitic marble, eastern China: Constraints on prograde, ultrahigh-pressure and retrograde metamorphic ages, *J. Metamorph. Geol.*, *24*, 569–589.

Mann, A., S. S. Hanna, and S. C. Nolan (1990), The post-Campanian tectonic evolution of the central Oman mountains: Tertiary extension of the eastern Arabian margin, in *The Geology and Tectonics of the Oman Region*, edited by A. H. F. Robertson, M. P. Searle, and A. Ries, *Geol. Soc. Spec. Publ.*, *49*, 549–564.

Michard, A., B. Goffé, and M. Ouazzani-Touhami (1983), Obduction related high pressure, low temperature metamorphism in upper crustal materials, Muscat, Oman, *Terra Cognita*, *3*, 22–23.

Michard, A., C. Chopin, and C. Henry (1993), Compression versus extension in the exhumation of the Dora-Maira coesite-bearing unit, Western Alps, Italy, *Tectonophysics*, *221*, 173–193, doi:10.1016/0040-1951(93)90331-D.

Michard, A., B. Goffé, O. Saddiqi, R. Oberhänsli, and A. S. Wendt (1994), Late Cretaceous exhumation of the Oman blueschists and eclogites: A two-stage extensional mechanism, *Terra Nova*, *6*, 404–413, doi:10.1111/j.1365-3121.1994.tb00514.x.

Miller, J. M., G. R. Gray, and R. T. Gregory (1998), Exhumation of high-pressure rocks in northeastern Oman, *Geology*, *26*, 235–238, doi:10.1130/0091-7613(1998)026<0235:EOHPRI>2.3.CO;2.

Miller, J. M., R. T. Gregory, D. R. Gray, and D. A. Foster (1999), Geological and geochronological constraints on the exhumation of a high-pressure metamorphic terrane, Oman, in *Exhumation Processes: Normal Faulting, Ductile Flow and Erosion*, edited by U. Ring et al., *Geol. Soc. Spec. Publ.*, *154*, 241–260.

Miller, J. M., G. R. Gray, and R. T. Gregory (2002), Geometry and significance of internal windows and regional isoclinal folds in northeast Saih Hatat, Sultanate of Oman, *J. Struct. Geol.*, *24*, 359–386, doi:10.1016/S0191-8141(01)00061-X.

Monié, P., and P. Agard (2009), Coeval blueschist exhumation along thousands of kilometers: Implications for subduction channel processes, *Geochem. Geophys. Geosyst.*, *10*, Q07002, doi:10.1029/2009GC002428.

Nicolas, A. (1989), *Structures in Ophiolites and Dynamics of Oceanic Lithosphere (Petrology and Structural Geology)*, Kluwer, Dordrecht, Germany.

O'Brien, P. (2006), Exhumation of UHP rocks: Deciphering the petrologic and geochronologic evidence in Himalayan examples, *Geophys. Res. Abstr.*, A-10573.

O'Brien, P. J., N. Zotov, R. Law, and A. M. Khan (2001), Coesite in Himalaya eclogite and implications for models of India-Asia collision, *Geology*, *29*, 435–438, doi:10.1130/0091-7613(2001)029<0435:CIHEAI>2.0.CO;2.

Omrani, J., P. Agard, H. Whitechurch, M. Benoit, G. Prouteau, and L. Jolivet (2008), Arc-magmatism and subduction history beneath Zagros: New report of adakites and geodynamic consequences, *Lithos*, *106*, 380–398, doi:10.1016/j.lithos.2008.09.008.

Parra, T., O. Vidal, and P. Agard (2002a), A thermodynamic model for Fe-Mg dioctahedral K white micas using data from phase-equilibrium experiments and natural pelitic assemblages, *Contrib. Mineral. Petrol.*, *143*, 706–732.

Parra, T., O. Vidal, and L. Jolivet (2002b), Relation between the intensity of deformation and retrogression in blueschist metapelites of Tinos Island (Greece) evidenced by chlorite-mica local equilibria, *Lithos*, *63*, 41–66, doi:10.1016/S0024-4937(02)00115-9.

Parra, T., O. Vidal, and T. Theye (2005), Experimental data on the Tschermak substitution in Fe-chlorite, *Am. Mineral.*, *90*, 359–370, doi:10.2138/am.2005.1556.

Parrish, R. R., S. J. Gough, M. P. Searle, and D. J. Waters (2006), Plate velocity exhumation of ultrahigh-pressure eclogites in the Pakistan Himalaya, *Geology*, *34*, 989–992, doi:10.1130/G22796A.1.

Pearce, J. A., T. Alabaster, A. W. Shelton, and M. P. Searle (1981), The Oman ophiolite as a Cretaceous arc-basin complex: Evidence and implications, in *Extensional Tectonics Associated With Convergent Plate Boundaries*, edited by F. J. Vine and A. G. Smith, *Philos. Trans. R. Soc. London, Ser. A*, *300*, 299–317.

Ricou, L. E. (1971), Le croissant ophiolitique péri-arabe, une ceinture de nappes mise en place au crétacé supérieur, *Rev. Geogr. Phys. Geol. Dyn.*, *13*, 327–350.

Rimmelé, G., T. Parra, B. Goffé, R. Oberhänsli, L. Jolivet, and O. Candan (2004), Exhumation paths of high-pressure-low-temperature metamorphic rocks from the Lycian nappes and Menderes Massif (SW Turkey): A multi-equilibrium approach, *J. Petrol.*, *46*, 641–669.

Robertson, A. H. F., and M. P. Searle (1990), The northern Oman Tethyan continental margin, in *The Geology and Tectonics of the Oman Region*, edited by A. H. F. Robertson, M. P. Searle, and A. C. Ries, *Geol. Soc. Spec. Publ.*, *49*, 3–25.

Rubatto, D., and J. Hermann (2001), Exhumation as fast as subduction?, *Geology*, *29*, 3–6, doi:10.1130/0091-7613(2001)029<0003:EAFAS>2.0.CO;2.

Scott, R. W. (1990), Chronostratigraphy of the Cretaceous carbonate shelf, southeastern Arabia, in *The Geology and Tectonics of the Oman Region*, edited by A. H. F. Robertson, M. P. Searle, and A. Ries, *Geol. Soc. Spec. Publ.*, *49*, 89–108.

Searle, M. P. (1985), Sequence of thrusting and origin of culminations in the northern and central Oman Mountains, *J. Struct. Geol.*, *7*, 129–143, doi:10.1016/0191-8141(85)90127-0.

Searle, M. P. (2007), Structural geometry, style and timing of deformation in the Hawasina Window, Jabal Al-Akhdar and Saih Hatat culminations, Oman Mountains, *GeoArabia*, *12*, 99–131.

Searle, M. P., and G. I. Alsop (2007), Eye-to-eye with a mega-sheath fold: A case study from Wadi Mayh, northern Oman Mountains, *Geology*, *35*, 1043–1046, doi:10.1130/G23884A.1.

Searle, M., and J. Cox (1999), Tectonic setting, origin, and obduction of the Oman ophiolite, *Geol. Soc. Am. Bull.*, *111*, 104–122, doi:10.1130/0016-7606(1999)111<0104:TSOAOO>2.3.CO;2.

Searle, M. P., and J. Cox (2002), Subduction zone metamorphism during formation and emplacement of the Semail ophiolite in the Oman Mountains, *Geol. Mag.*, *139*, 241–255, doi:10.1017/S0016756802006532.

Searle, M. P., and J. Malpas (1980), The structure and metamorphism of rocks beneath the Semail ophiolite of Oman and their significance in ophiolite obduction, *Trans. R. Soc. Edinburgh Earth Sci.*, *71*, 247–262.

Searle, M. P., and J. Malpas (1982), Petrochemistry and origin of sub-ophiolite metamorphic and related rocks in the Oman Mountains, *J. Geol. Soc.*, *139*, 235–248, doi:10.1144/gsjgs.139.3.0235.

Searle, M. P., D. J. Waters, H. N. Martin, and D. C. Rex (1994), Structure and metamorphism of blueschist-eclogite facies rocks from the northeastern Oman Mountains, *J. Geol. Soc.*, *151*, 555–576, doi:10.1144/gsjgs.151.3.0555.

Searle, M. P., C. J. Warren, D. J. Waters, and R. R. Parrish (2004), Structural evolution, metamorphism and restoration of the Arabian continental margin, Saih Hatat region, Oman Mountains, *J. Struct. Geol.*, *26*, 451–473, doi:10.1016/j.jsg.2003.08.005.

Searle, M. P., C. J. Warren, D. J. Waters, and R. R. Parrish (2005), Reply to: Comment by Gray, Gregory and Miller on "Structural evolution, metamorphism and restoration of the Arabian continental margin, Saih Hatat region, Oman Mountains," *J. Struct. Geol.*, *27*, 375–377, doi:10.1016/j.jsg.2004.07.003.

Shervais, J. W. (2001), Birth, death, and resurrection: The life cycle of suprasubduction zone ophiolites, *Geochem. Geophys. Geosyst.*, *2*, 1010, doi:10.1029/2000GC000080.

Trotet, F., O. Vidal, and L. Jolivet (2001), Exhumation of Syros and Sifnos metamorphic rocks (Cyclades, Greece): New constraints on the P-T paths, *Eur. J. Mineral.*, *13*, 901–920, doi:10.1127/0935-1221/2001/0013/0901.

Vidal, O., and T. Parra (2000), Exhumation paths of high-pressure metapelites obtained from local equilibria for chlorite-phengite assemblages, *Geol. J.*, *35*, 139–161, doi:10.1002/gj.856.

Vidal, O., and T. Theye (1996), Petrology of Fe-Mg-carpholite-bearing metasediments from NE Oman, *J. Metamorph. Geol.*, *14*, 381–397.

Vidal, O., B. Goffé, and T. Theye (1992), Experimental study of the stability of sudoite and magnesiocarpholite and calculation of a new petrogenetic grid for the system FeO-MgO-Al$_2$O$_3$-SiO$_2$-H$_2$O, *J. Metamorph. Geol.*, *10*, 603–614, doi:10.1111/j.1525-1314.1992.tb00109.x.

Vidal, O., T. Parra, and F. Trotet (2001), A thermodynamic model for Fe-Mg aluminous chlorite using data from phase equilibrium experiments and natural pelitic assemblages in the 100° to 600°C, 1 to 25 kb range, *Am. J. Sci.*, *301*, 557–592, doi:10.2475/ajs.301.6.557.

Vidal, O., T. Parra, and P. Vieillard (2005), Thermodynamic properties of the Tschermak solid solution in Fe-chlorite: Application to natural examples and possible role of oxidation, *Am. Mineral.*, *90*, 347–358, doi:10.2138/am.2005.1554.

Vidal, O., V. De Andrade, E. Lewin, M. Munoz, T. Parra, and S. Pascarelli (2006), P-T-deformation-Fe^{3+}/Fe^{2+} mapping at the thin section scale and comparison with XANES mapping: Application to a garnet-bearing metapelite from the Sambagawa

metamorphic belt (Japan), *J. Metamorph. Geol.*, *24*, 669–683.

Wain, A. (1997), New evidence for coesite in eclogite and gneisses: Defining an ultra-high pressure province in the Western Gneiss Region of Norway, *Geology*, *25*, 927–930, doi:10.1130/0091-7613(1997) 025<0927:NEFCIE>2.3.CO;2.

Warburton, J., T. J. Burnhill, R. H. Graham, and K. P. Isaac (1990), The evolution of the Oman Mountains foreland basin, in *The Geology and Tectonics of the Oman Region*, edited by A. H. F. Robertson, M. P. Searle, and A. Ries, *Geol. Soc. Spec. Publ.*, *49*, 419–427.

Warren, C. J., and J. M. Miller (2007), Structural and stratigraphic controls on the origin and tectonic history of a subducted continental margin, Oman, *J. Struct. Geol.*, *29*, 541–558, doi:10.1016/j.jsg. 2006.10.006.

Warren, C. J., and D. J. Waters (2006), Oxidized eclogites and garnet-blueschists from Oman: *P-T* path modelling in the NCFMASHO system, *J. Metamorph. Geol.*, *24*, 783–802.

Warren, C. J., R. R. Parrish, M. P. Searle, and D. J. Waters (2003), Dating the subduction of the Arabian continental margin beneath the Semail ophiolite, Oman, *Geology*, *31*, 889–892, doi:10.1130/ G19666.1.

Warren, C. J., R. R. Parrish, D. J. Waters, and M. P. Searle (2005), Dating the geologic history of Oman's Semail ophiolite: Insights from U-Pb geochronology, *Contrib. Mineral. Petrol.*, *150*, 403–422, doi:10.1007/s00410-005-0028-5.

Willner, A. P., J. Glodny, T. V. Gerya, E. Godoy, and H.-J. Massonne (2004), A counterclockwise *PTt* path of high-pressure/low-temperature rocks from the Coastal Cordillera accretionary complex of south-central Chile: Constraints for the earliest stage of subduction mass flow, *Lithos*, *75*, 283–310, doi:10.1016/j.lithos.2004.03.002.

Yamato, P., P. Agard, B. Goffé, V. De Andrade, O. Vidal, and L. Jolivet (2007), New, high-precision *P-T* estimates for Oman blueschists: Implications for obduction, nappe stacking and exhumation

processes, *J. Metamorph. Geol.*, *25*, 657–682, doi:10.1111/j.1525-1314.2007.00722.x.

Zhang, R. Y., J. G. Liou, W. G. Ernst, R. G. Coleman, N. V. Sobolev, and V. S. Shatsky (1997), Metamorphic evolution of diamond-bearing and associated rocks from the Kokchetav Massif, northern Kazakhstan, *J. Metamorph. Geol.*, *15*, 479–496, doi:10.1111/j.1525-1314.1997.00035.x.

───────────

P. Agard, ISTEP, UMR 7193, UPMC Paris 06, CNRS, F-75005, Paris, France. (philippe.agard@upmc.fr)

G. I. Alsop, Department of Geology and Petroleum Geology, School of Geosciences, University of Aberdeen, Aberdeen AB24 3UE, UK.

B. Dubacq, Department of Earth Sciences, Cambridge University, Downing Street, Cambridge CB2 3EQ, UK.

M. P. Searle, Department of Earth Sciences, Oxford University, Parks Road, Oxford OX1 3PR, UK.